Stellar Orbital Studies in Normal Spiral Galaxies II: Restrictions to Structural and Dynamical parameters on Spiral Arms

A. Pérez-Villegas[1], B. Pichardo[2], E. Moreno[2]

[1] *Max-Planck-Institüt für Extraterrestrische Physik, Gießenbachstraße, 85748 Garching, Germany;*
mperez@mpe.mpg.de

[2] *Instituto de Astronomía, Universidad Nacional Autónoma de México, A.P. 70–264, 04510, México, D.F.; Universitaria, D.F., México*

ABSTRACT

Making use of a set of detailed potential models for normal spiral galaxies, we analyze the disk stellar orbital dynamics as the structural and dynamical parameters of the spiral arms (mass, pattern speed and pitch angle) are gradually modified. With this comprehensive study of ordered and chaotic behavior, we constructed an assemblage of orbitally supported galactic models and plausible parameters for orbitally self-consistent spiral arms models. We find that, to maintain orbital support for the spiral arms, the spiral arm mass, M_{sp}, must decrease with the increase of the pitch angle, i; if i is smaller than $\sim 10°$, M_{sp} can be as large as $\sim 7\%$, $\sim 6\%$, $\sim 5\%$ of the disk mass, for Sa, Sb, and Sc galaxies, respectively. If i increases up to $\sim 25°$, the maximum M_{sp} is $\sim 1\%$ of the disk mass independently in this case of morphological type. For values larger than these limits, spiral arms would likely act as transient features. Regarding the limits posed by extreme chaotic behavior, we find a strong restriction on the maximum plausible values of spiral arms parameters on disk galaxies beyond which, chaotic behavior becomes pervasive. We find that for i smaller than $\sim 20°$, $\sim 25°$, $\sim 30°$, for Sa, Sb, and Sc galaxies, respectively, M_{sp} can go up to $\sim 10\%$, of the mass of the disk. If the corresponding i is around $\sim 40°$, $\sim 45°$, $\sim 50°$, M_{sp} is $\sim 1\%$, $\sim 2\%$, $\sim 3\%$ of the mass of the disk. Beyond these values, chaos dominates phase space, destroying the main periodic and the neighboring quasi-periodic orbits.

Subject headings: Chaos – galaxies: evolution – galaxies: kinematics and dynamics – galaxies: spiral – galaxies: structure

1. Introduction

With the advent of the new extended and profound surveys of the Galaxy and other galaxies, we will likely understand much more of spiral galaxy morphology and kinematics with unprecedented

detail. At this moment however, our understanding of splendid structures in galaxies, such as the spiral arms, is quite limited; including for example, its very nature and origin, how they are supported, whether they are long lasting or transient, if they exhibit noticeable (observable) effects on the stellar and gaseous dynamics behavior, what are their orbital effects in different types of spirals, etc.

The first firm step into the path of understanding the Milky Way and spiral galaxies in general was given by morphological classifications, that have provided important statistical information about their structural parameters, such as luminosity ratios of their main components (bulge, disk, and nonaxisymmetric large scale features: bars, spiral arms, rings, etc.), rotation curve, spiral-arms pitch angles, etc. The first morphological classification that tried to taxonomize galaxies was the Hubble sequence (Hubble 1926, 1936). This represents the simplest classification scheme and within it, the normal spiral galaxies, in which we focus this work, range from 'early' to 'late' (Sa to Sc), mainly based on two criteria: the pitch angle of spiral arms and the bulge-to-disk luminosity ratio. An Sa galaxy possesses smoother closed spiral arms and a conspicuous central bulge, an Sc galaxy has open and remarkably structured spiral arms and a small central bulge, an Sb galaxy is intermediate between both types. Although the Hubble morphological classification is satisfactory for galaxies with redshift $z < 0.5$ (van den Bergh 2002), where non-interacting galaxies have had time to relax, it is well known that this scheme does not fully comprises all galaxies. Indeed, structural parameters of disks present a large scatter among catalogued galaxies with the same morphological type. The best example of this is the pitch angle, that ranges from about $8°$ to $50°$ (Kennicutt 1981; Ma et al. 2000; Davis et al. 2012) for late type galaxies, for instance.

Some recent studies present spiral arms as likely transient features from simulations (D'Onghia et al. 2013; Baba et al. 2013; Grand et al. 2012a,b; Roškar et al. 2012; Wada et al. 2011; Sellwood 2011; Fujii et al. 2011; Dobbs & Bonnell 2006), or transient as a product of overlapping of multiple spiral modes coupled together through resonances at the corotation radius (Sellwood & Carlberg 2014; Roškar et al. 2012; Quillen et al. 2011). Spiral arms have also been found to corotate with the disk (i.e. winding up, therefore transient ; Roca-Fàbrega et al. 2013; Kawata et al. 2014). Also, from the observational point of view there seem to be evidences of transient spiral arms (Speights & Westpfahl 2011, 2012; Ferreras et al. 2012; Foyle et al. 2011; Meidt et al. 2008; Meidt et al. 2009; Merrifield et al. 2006). On the other hand, observational and theoretical evidences of the opposite, i.e., long-lived spiral arms, has been presented (Scarano & Lépine 2013; Cedrés et al. 2013; Martínez-García & González-Lopezlira 2013; Law et al. 2012; Scarano et al. 2011; Sánchez-Gil et al. 2011; Egusa et al. 2009; Grosbøl & Dottori 2009; Zhang 1998; Donner & Thomasson 1994; Efremov 1985). Whether spiral arms are all transient features, or in some cases they could be long-lasting, remains still a polemic matter in modern astrophysics.

In previous studies (Pérez-Villegas et al. 2013, hereafter Paper I, and Pérez-Villegas et al. 2012), we employed the ideal Hubble classification scheme as the base to construct the axisymmetric background gravitational potential models for spiral galaxies (i.e. bulge, disk and halo). With this set of models, we analyzed the stellar orbital dynamics on disks, produced by spiral arms in

different galactic morphological types. The constructed galactic potential models then follow the typical morphology that characterizes the Hubble sequence in terms of the rotation curve, bulge-to-disk mass ratios and scale-lengths. These studies were performed on steady, realistic potentials for spiral galaxies. These type of potentials can not follow the galactic evolution, but they are able to provide some restrictions of potentials based on the detailed structure of orbital chaos, and on the existence and structure of periodic orbits as the dynamical support to shape stellar systems. The main purpose of our study has been to disentangle all possible details of the orbital structure, which are not straightforward to discern yet on N-body simulations.

Using these models, we performed an extensive study of the pitch angle in normal spiral galaxies. We run thousands of orbits for different timescales depending on the specific problem. Two restrictions to the spiral arms structure were imposed theoretically; one on their steady or transient nature and the other on their maximum pitch angle prior to destruction. The first restriction is based on the orbital ordered behavior, where we found a maximum pitch angle of $\sim 15°$, $\sim 18°$ and $\sim 20°$ for Sa, Sb and Sc spiral galaxies, respectively. Up to these limits the density response supports closely the imposed spiral arms at all radii, the spiral arms are stable, and could be of long-lasting nature. Galaxies with spiral arms having pitch angles beyond these limits would rather be explained as transient features. The second restriction is based on chaotic orbital behavior; in this case the limits for the pitch angle are $\sim 30°$, $\sim 40°$ and $\sim 50°$ for Sa, Sb and Sc spiral galaxies, respectively. Beyond these limits, chaos becomes pervasive wiping out the spiral arms.

In the present analysis we continue our extensive stellar dynamical studies in normal spiral galaxies, from early to late types, but now we cover all the most important spiral arms parameters that include: arms total mass (relative to the disk), angular velocity, and pitch angle interrelated. We produce experiments exploring the statistical effect on stellar orbits on the galactic plane due to the variations of these parameters. The main objectives of this work are (1) to elucidate the influence of spiral arms on different morphological types of galaxies, as going from early to late types, (2) to provide some restrictions to structural and dynamical parameters of galaxies, and (3) to produce a set of parameters for 'allowed spiral models', which are self-consistent from an orbital (periodic orbits) point of view, with good probabilities of being long-lasting structures, and with mild or quiet chaotic nature. With these parameters, steady models can be constructed that result in likely robust and persisting entities.

This paper is organized as follows. The galactic potential and the methodology are described in Section 2. The effect on the disk dynamics, due to the variation of the spral arms mass and their angular velocity in different morphological types (Sa, Sb and Sc galaxies) is presented in Section 3. In Section 4, we present a valid set of structural and dynamical parameters for plausible long-lasting spiral arms nature, and also their maximum values before chaos dominates. In Section 5 we discuss the effect of structural and dynamical parameters of spiral arms (pitch angle, angular speed, and mass) in normal spiral galaxies and present our conclusions.

2. Numerical Implementation and Methodology

With the use of the observationally motivated family of models for normal spiral galactic potentials presented in Paper I, we performed a comprehensive stellar orbital dynamics study. The main tools employed for this task are periodic orbits, density response calculations, and phase-space (Poincaré) diagrams. The potential of each galaxy is formed by an axisymmetric part, plus a nonaxisymmetric potential represented by a detailed model of the spiral arms. In the following, we summarize some properties of the galactic models and the employed tools.

2.1. Models for Normal Spiral Galaxies

The galactic models consist of axisymmetric and nonaxisymmetric parts. The axisymmetric part is formed by a bulge and disk of the form proposed by Miyamoto-Nagai (1975), and a massive spherical halo (Allen & Santillán 1991). With these components, in Paper I we fit the different galaxy types considering the typical rotation curves for Sa, Sb and Sc galaxies, and the bulge-to-disk mass ratios (see Figure 1 of Paper I). The nonaxisymmetric part is the three-dimensional model of spiral arms given by Pichardo et al. 2003, called PERLAS. This model is a mass distribution formed by a set of inhomogeneous oblate spheroids lying on a logarithmic spiral locus; it has been tested and compared with other theoretical models (Martos et al. 2004; Antoja et al. 2009, 2011).

In Table 1 we present the observational and theoretical parameters employed to fit the galactic models and their respective references (data taken from Paper I). In this table, D, B, H, refer to the disk, bulge, and halo components, respectively; M_{sp} is the total mass of the spiral arms, i is their pitch angle, and Ω_p is their angular speed. In our models we take a clockwise rotation. To simplify the notation, in the following we call $\mu = M_{sp}/M_D$, i.e., the ratio of the mass of the spiral arms to the mass of the disk.

In our models, regarding the radial extent of the spiral arms, we consider as their initial and final galactocentric radii the inner Lindblad resonance (ILR) and the corotation resonance (CR), respectively. This is based on theoretical studies of orbital self-consistency of spiral arms (Contopoulos & Grosbøl 1986, 1988; Patsis et al. 1991; Pichardo et al. 2003). In Table 2 we present the positions of the main resonances ILR, 4/1, and CR for normal spiral galaxies (from early to late types). With a clockwise rotation for the disk, we assume Ω_p between 10 and $60 \, \mathrm{km \, s^{-1} \, kpc^{-1}}$, independently of the Hubble type.

For the mass of the spiral arms, we explore its orbital effect in the range from 1% to 10% of the total disk mass, i.e., μ between 0.01 and 0.1, independently of the Hubble type. On the other hand, the spiral arms strength depends mainly on two parameters, their mass and pitch angle. To measure this strength and assure that our parameters are within observational limits, we have employed the Q_T parameter (Combes & Sanders 1981). This parameter Q_T is defined as

Table 1.   Parameters of the Axisymmetric Potential

Parameter	Value			Reference
		Spiral Arms		
	Sa	Sb	Sc	
Locus		Logarithmic		1,9,10
Arms Number		2		2
Pitch Angle i (°)	$7 - 20$	$10 - 20$	$15 - 30$	3,7
$\mu = \mathrm{M_{sp}/M_D}$		$0.01 - 0.10$		
Scale-Length (kpc)	7	5	3	Disk based
Ω_p [1] (km s^{-1} kpc^{-1})		10 to 60		1,6
	Axisymmetric Components			
$\mathrm{M_D/M_H}$ [2]	0.07	0.09	0.1	4,8
$\mathrm{M_B/M_D}$	0.9	0.4	0.2	5,8
Rotation Velocity [3] (km s^{-1})	320	250	170	7
$\mathrm{M_D}$ ($10^{10}\mathrm{M_\odot}$)	12.8	12.14	5.10	4
$\mathrm{M_B}$ ($10^{10}\mathrm{M_\odot}$)	11.6	4.45	1.02	$M_\mathrm{B}/M_\mathrm{D}$ based
$\mathrm{M_H}$ ($10^{11}\mathrm{M_\odot}$)	16.4	12.5	4.85	$M_\mathrm{D}/M_\mathrm{H}$ based
Disk Scale-Length (kpc)	7	5	3	4,5
	Constants of the Axisymmetric Components [4]			
Bulge $(\mathrm{M_B}, \mathrm{b_1})$ [5]	5000, 2.5	2094.82, 1.7	440, 1.0	
Disk $(\mathrm{M_D}, \mathrm{a_2}, \mathrm{b_2})$ [5]	5556.03, 7.0, 1.5	5232.75, 5.0, 1.0	2200, 5.3178, 0.25	
Halo $(\mathrm{M_H}, \mathrm{a_3})$ [5]	15000, 18.0	10000, 16.0	2800, 12.0	

[1]The rotation of the spiral arms is clockwise.

[2]Up to 100 kpc halo radius.

[3]V_{max}.

[4]In galactic units, where a galactic mass unit $= 2.32 \times 10^7$ M$_\odot$ and a galactic distance unit $=$ kpc.

[5]b$_1$, a$_2$, b$_2$, and a$_3$ are scale lengths.

References. — (1) Grosbøl & Patsis 1998; (2) Drimmel et al. 2000; Grosbøl et al. 2002; Elmegreen & Elmegreen 2014; (3) Kennicutt 1981; (4) Pizagno et al. 2005; (5) Weinzirl et al. 2009; (6) Patsis et al. 1991; Grosbøl & Dottori 2009; Egusa et al. 2009; Fathi et al. 2009; Gerhard 2011; (7) Brosche 1971; Ma et al. 2000; Sofue & Rubin 2001; (8) Block et al. 2002; (9) Pichardo et al. 2003; (10) Seigar & James 1998; Seigar et al. 2006.

$$Q_{\mathrm{T}}(R) = F_T^{\mathrm{max}}(R)/|\langle F_{\mathrm{R}}(R)\rangle|, \tag{1}$$

where $\mathrm{F}_T^{\mathrm{max}}(\mathrm{R}) = |\left(\frac{1}{R}\ \partial\Phi(\mathrm{R},\theta)/\partial\theta\right)|_{\mathrm{max}}$, is the maximum amplitude of the tangential force at galactocentric radius R, and $\langle\mathrm{F_R(R)}\rangle$, is the average axisymmetric radial force at the same radius, derived from the m = 0 Fourier component of the gravitational potential.

In Figure 1a we show the maximum value, $(\mathrm{Q_T})_{\mathrm{max}}$, of the parameter Q_T for each galaxy type (Sa, Sb and Sc), as we increase the pitch angle i from $0°$ to $90°$. For this figure we employed the maximum plausible value of μ (i.e. before chaos dominates the phase space surrounding the families of orbits that support the pattern; see Section 3), of 0.1, 0.07, and 0.05, for Sa, Sb and Sc galaxies, respectively. In our study, taking i between $7°$ and $30°$ (Table 1) and using the maximum limits of the mass of the spiral arms, $(\mathrm{Q_T})_{\mathrm{max}}$ is not larger than ~ 0.25. From the literature, reasonable maximum values for Q_T are ~ 0.2 for early spirals and ~ 0.3 for late spirals (Buta et al. 2005), therefore, our models are within observational limits.

In Figure 1b we show $(\mathrm{Q_T})_{\mathrm{max}}$ for each galaxy type as we increase μ from 0.01 to 0.1. In this figure we have considered the value of i before chaos dominates the available phase space, which corresponds to $\sim 30°$, $\sim 40°$ and $\sim 50°$, for Sa, Sb and Sc galaxies, respectively (see Section 3). For Sa and Sb models, $(\mathrm{Q_T})_{\mathrm{max}}$ increases much slower than for the Sc ones. In early galaxy type models very massive spiral arms are allowed within this observational restriction without exceeding observational limits, even for spiral arms with $\mu = 0.1$; see for example (Weiner & Sellwood 1999). For the Sc type, $(\mathrm{Q_T})_{\mathrm{max}}$ increases much faster with mass, and for approximately $\mu > 0.06$ the spiral arms strength increases $((\mathrm{Q_T})_{\mathrm{max}} > 0.3)$ more than what observations indicate for this type of galaxies.

2.2.   Tools for the Orbital Analysis

For the orbital dynamics analysis we employed periodic orbits and Poincaré diagrams. We have also calculated the density response as in Paper I, using the method of Contopoulos & Grosbøl (1986), which quantifies the support of spiral arms with periodic orbits. This method to estimate the density response has been widely used in literature (Contopoulos & Grosbøl 1988; Amaral & Lepine 1997; Yano et al. 2003; Pichardo et al. 2003; Voglis et al. 2006; Tsoutsis et al. 2008; Pérez-Villegas et al. 2012, 2013; Junqueira et al. 2013). We computed between 40 and 60 periodic orbits for each galactic model. The density response is defined as the regions where periodic orbits crowd producing a density enhancement. The position of the maximum density response along each periodic orbit is calculated, and with these positions the locus formed by the maxima of density response is found and compared with the position of the imposed spiral locus (i.e. PERLAS). The method implicitly considers a small and variable dispersion since it studies a region where the flux is conserved. Additionally, we estimated the average density response around each one of
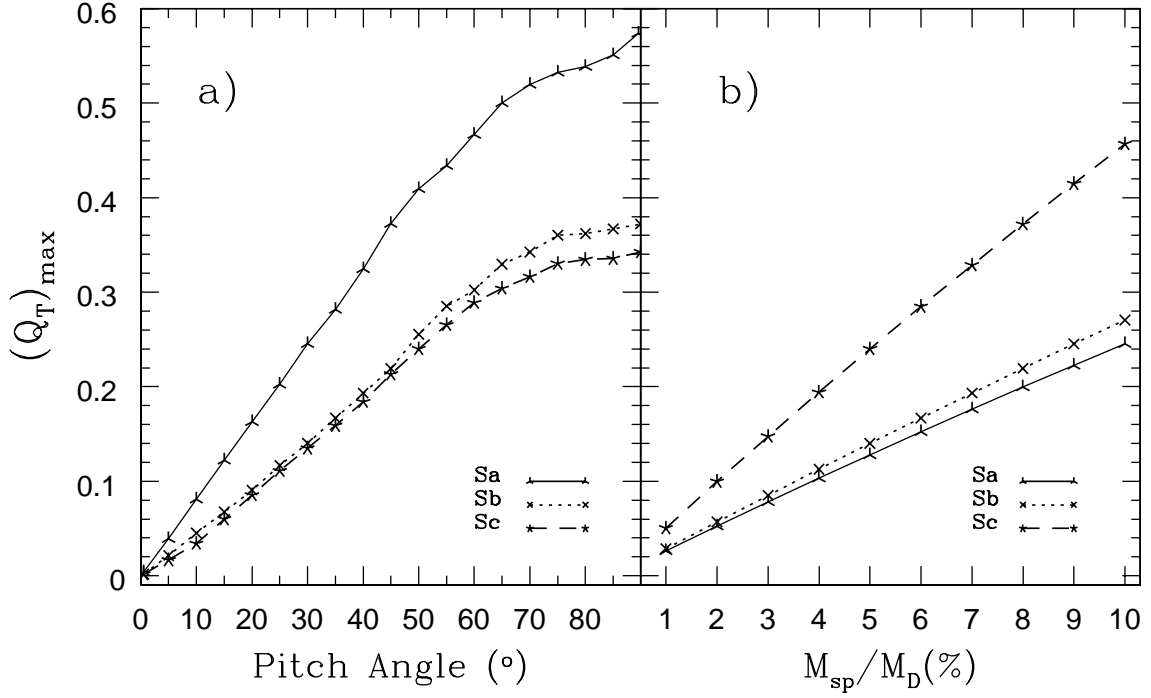
Fig. 1.— Maximum value, $(Q_T)_{max}$, of the parameter $Q_T(R)$. The continuous, dotted, and dashed lines give $(Q_T)_{max}$ for an Sa, Sb, and Sc galaxy, respectively. In $a)$, we show $(Q_T)_{max}$ vs. pitch angle of the spiral arms, i, where $\mu = M_{sp}/M_D = 0.1$, 0.07, and 0.05 for Sa, Sb and Sc, respectively. In $b)$, we show $(Q_T)_{max}$ vs. μ, where the pitch angle is 30°, 40° and 50° for Sa, Sb and Sc, respectively.

these maxima response. In order to do that, we took a circular vicinity, and compared the density response with the imposed density (this is the sum of the axisymmetric disk density on the galactic plane and the central density of the spiral arms).

Regarding the Poincaré diagrams, these are constructed in the plane (x', v_x'), in the non-inertial reference system that rotates with the spiral arms. The x' axis points toward the direction of the line where the spiral arms begin in the inner galactic region. Poincaré diagrams have two regions: the prograde region, where the stars move in the same direction of rotation of the spiral arms, and the retrograde region, where the stars move in opposite direction to the spiral arms rotation. These regions (prograde and retrograde) were defined in the non-inertial frame where the spiral arms are at rest. In our models the rotation of the spiral arms is clockwise, thus, the left side of the diagram is prograde (launching orbits with $x' < 0, v_y' > 0$), and the right side is retrograde (with $x' > 0, v_y' > 0$). Ordered orbits are shown as one-dimensional curves, periodic orbits as a few set of dots (one single dot represents the strongest periodic orbits, surrounded by other ordered, quasi-periodic and periodic orbits of lower order), and chaotic orbits are seen as scattered sets of points. The chaotic regions may surround periodic orbits, and confined chaotic orbits is able to support large-scale structures such as spiral arms (Patsis & Kalapotharakos 2011; Kaufmann & Contopoulos 1996; Contopoulos & Grosbøl 1986). However, an excess of chaos would start making it difficult for orbits to support structures, until chaos is not confined anymore, destroying large scale patterns (chaos in this case penetrates up to the X_1 periodic orbits regions). Large-scale structures are not expected to arise from systems fully dominated by chaos (Voglis et al. 2006). The most interesting part of the phase space diagrams is the prograde region where the great majority of stars are moving in spiral galaxies. Chaos is generated in this region, mostly due to resonance overlapping (Martinet 1974; Athanassoula et al. 1983 and references therein). In the retrograde region, the resonances are very separated, thus the production of chaos is almost null. Each Poincaré diagram contains 50 orbits, distributed between the prograde and retrograde regions, with 300 points each (points correspond to the numbers of periods). For more details about this methodology (periodic orbits, density response and phase-space diagrams), see Paper I.

3. Orbital Study of Ordered and Chaotic Behavior

With the methodology described in the previous section, we have carried out a detailed orbital study with periodic orbits, density response calculations, and phase space diagrams. With all these tools we try to determine whether limiting values to different structural and dynamical parameters of normal spiral galaxies can be established. In Paper I we found two limits to the pitch angle i for normal spiral galaxies (Sa, Sb and Sc); in the present study we set limits to combinations of the spiral arms-to-disk mass ratio, μ, the angular velocity of the spiral arms, Ω_p, combined with the pitch angle, i, in order to seek for plausible long-term spiral galactic models. By plausible and long-lasting in this context, we mean spiral arms fully supported by periodic orbits and moderate production of chaotic behavior.

To measure observationally both the mass and angular velocity of spiral arms is not an easy task. We have tried instead to constrain these parameters through the orbital support of the spiral arms with periodic orbits (ordered behavior), and with the study of chaotic behavior with Poincaré diagrams, by searching for a limit before chaos dominates the available phase space and destroys periodic orbits.

We present in this section a family of orbitally plausible long-lasting spiral galactic potentials, and provide optimal ranges for the parameters i, $\Omega_{\rm p}$, and μ.

3.1. Analyzing the Effect of the Spiral Arms Mass: Ordered and Chaotic Behavior

We performed an exhaustive study of periodic orbits for different morphological galactic types. With the maps of periodic orbits we found the position of the maximum density response along each periodic orbit, and in order to analyze some orbital self-consistency of the spiral arms, these positions were compared with the center of the imposed spiral pattern. If the imposed spiral arms are supported by the maxima of density response, then these arms are stable and are of a long-lasting nature. If this condition is not satisfied, the spiral arms might be rather explained as transient structures.

For each morphological type, we used the corresponding axisymmetric background potential, based on the parameters presented in Table 1. In order to dilucidate the relative importance of the different parameters, we present in this section several examples first. μ has been varied from 0.01 to 0.1, and the representative employed pitch angles i are taken as $10°$, $15°$ and $20°$, for Sa, Sb and Sc galaxies, respectively. Additionally, in our computations we have varied slightly $\Omega_{\rm p}$ in each galactic type.

In Figure 2, for an Sa galaxy with $i = 10°$, we show in the galactic plane x', y' the maxima of density response, with filled squares, which correspond to crowding regions of periodic orbits (black curves) that produce density enhancements; the center of the imposed spiral arms potential (PER-LAS model) is shown with open squares and the dotted lines mark the width of spiral arms. From top to bottom panels (the x' axis is at the bottom), $\Omega_{\rm p}$ lies in the interval $[20, 40]$ km s^{-1} kpc^{-1}, and the values of μ are marked at the top. In each panel we show with red, blue, and yellow circles the positions of the resonances ILR, 4/1 and CR; see Table 2. This figure shows that the maxima of density response coincide well (within $3°$ difference) with the imposed spiral arms, but the extent of this density support reduces significantly for the largest values of μ, reaching only up to the 4/1 resonance if μ is around 0.1. Also, the density support diminishes strongly if $\Omega_{\rm p}$ increases.

In Figure 3 we consider $i = 20°$ in an Sa type galaxy. In this case the orbital dynamics is strongly affected. The density response systematically forms spiral arms with a smaller pitch angle than the imposed $20°$, and with a reduced radial extent compared with the case $i = 10°$. The partial density support is destroyed when $\Omega_{\rm p}$ increases. Spiral arms with this strong forcing in a galaxy, might be better explained as transient structures. In Paper I we found that the regime

where the spiral arms of Sa galaxies are transient occurs when $i \gtrsim 15°$.

Figures 4 and 5 show our results for an Sb galaxy with pitch angles $i = 15°$ and $i = 20°$, respectively. In these cases Ω_p lies in the interval $[15, 35]$ km s^{-1} kpc^{-1}. These figures show a similar behavior to the case of an Sa galaxy, but it was harder to obtain a reasonable density support for larger values of μ. With the greater value $i = 20°$, the resulting response pitch angle is slightly smaller than the imposed $20°$.

Our results for an Sc galaxy are shown in Figures 6 and 7, with pitch angles $i = 20°$ and $i = 30°$, respectively. Ω_p lies in the interval $[10, 30]$ km s^{-1} kpc^{-1}. We do not find a density support toward the greatest values of μ and Ω_p, and for their smallest values the response density shows a pitch angle smaller than the imposed one. The radial extent of this response shortens compared with that obtained in Sa and Sb types.

In order to complement and to reinforce the results obtained by the construction of periodic orbits, in Figures 8 -13, we have compared the spiral arm density response (filled squares) with the spiral arms imposed density (PERLAS, open squares). Each mosaic of density response (Figures 8 -13) corresponding to each periodic orbit mosaic (Figures 2 -7). In Figure 8, we present densities for an Sa galaxy with $i = 10°$. As the maximum density response was shown in Figure 2, this figure presents that for μ up to ~ 0.05, the density response fits well with the imposed density. Figure 9 shows also a Sa galaxy, but with $i = 20°$, in this case the spiral arms are stronger, and we see that density response fits to imposed density with a smaller μ. Therefore, if the pitch angle increases, the allowed mass in spiral arms should be smaller, in order to maintain the orbital support and the density response fits better to the imposed density.

Figures 10 and 11 show density response for an Sb galaxy with pitch angles $i = 15°$ and $i = 20°$, respectively. In these figures we see a similar behavior than for Sa galaxies. The density response in this case, fits the imposed density up to $\mu \sim 0.03$, but if the pitch angle increases, the value of μ is affected.

Figures 12 and 13 show densities for an Sc galaxy with pitch angles $i = 20°$ and $i = 30°$, respectively. In these figures we see a similar behavior than in Sa and Sb galaxies. We can notice that the density response fits to imposed density up to $\mu \sim 0.03$. For larger values of μ and Ω_p, the density support is not found.

Figures 8 -13, show that the response is compatible with the imposed densities up to a certain limit in mass. The larger the force of the spiral arms, the stronger the response relative to the imposed one. It is worth noticing that, this over-response does not indicate that the model is inconsistent as long as the response is in phase. Rather, it would indicate a growing mode, which would be probably damped by an increase in velocity dispersion, if feedback were included in a totally self-consistent model.

Now, in order to study the chaotic behavior, we produced a comprehensive study of Jacobi energy (E_J) families in phase space, from very bounded orbits (the inner part of galaxy) to the
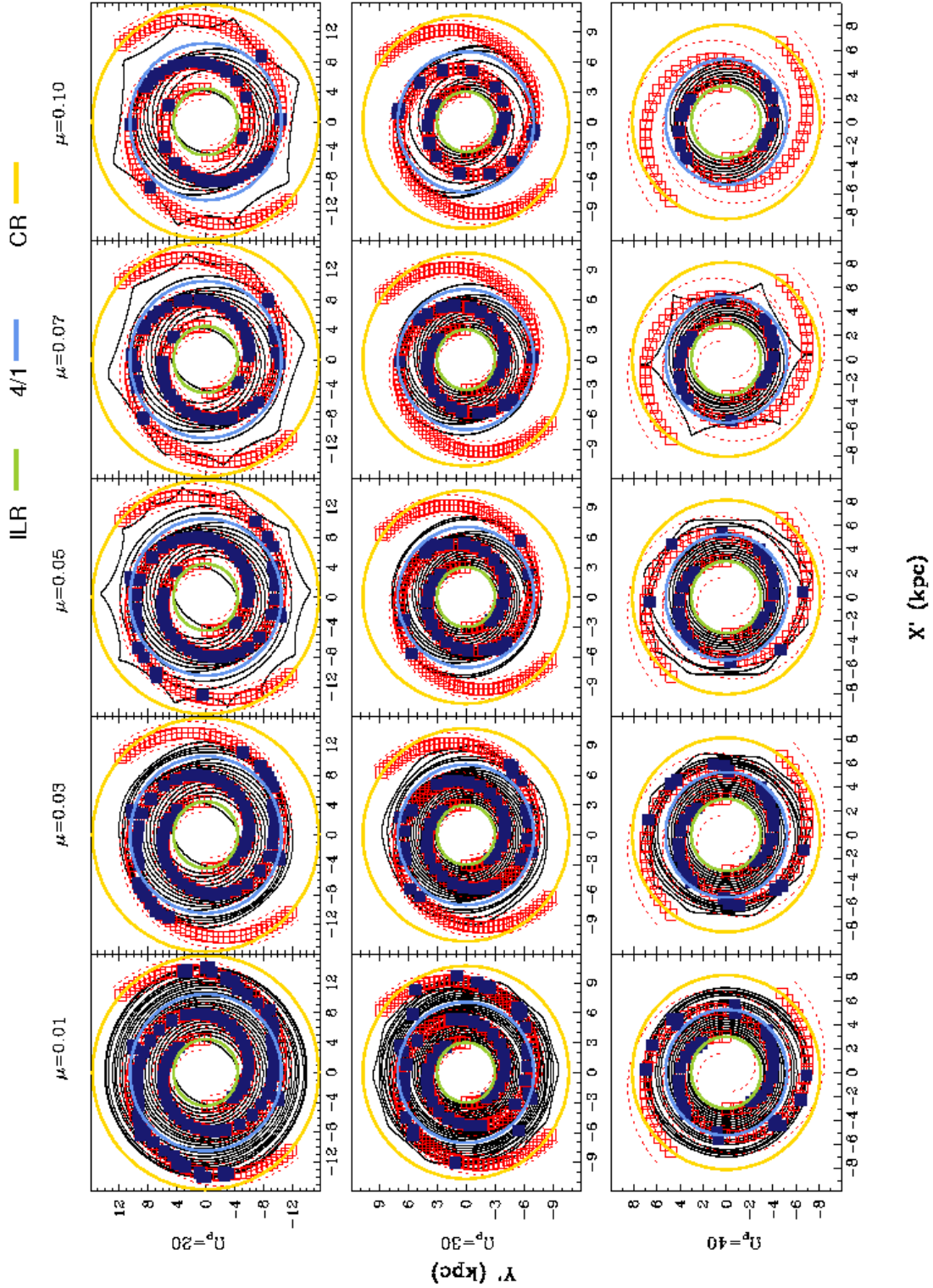
Fig. 2.— Periodic orbits (black curves), density response maxima (filled squares), and the imposed spiral arms locus (open squares and dotted lines mark the width of spiral arms) for the three-dimensional spiral arms model of an Sa galaxy with a pitch angle $i = 10°$. The values of $\mu = M_{\rm sp}/M_{\rm D}$ and the angular speed of the spiral arms, $\Omega_{\rm p}$ in units of km s^{-1} kpc^{-1}, are given at the top and left, respectively.
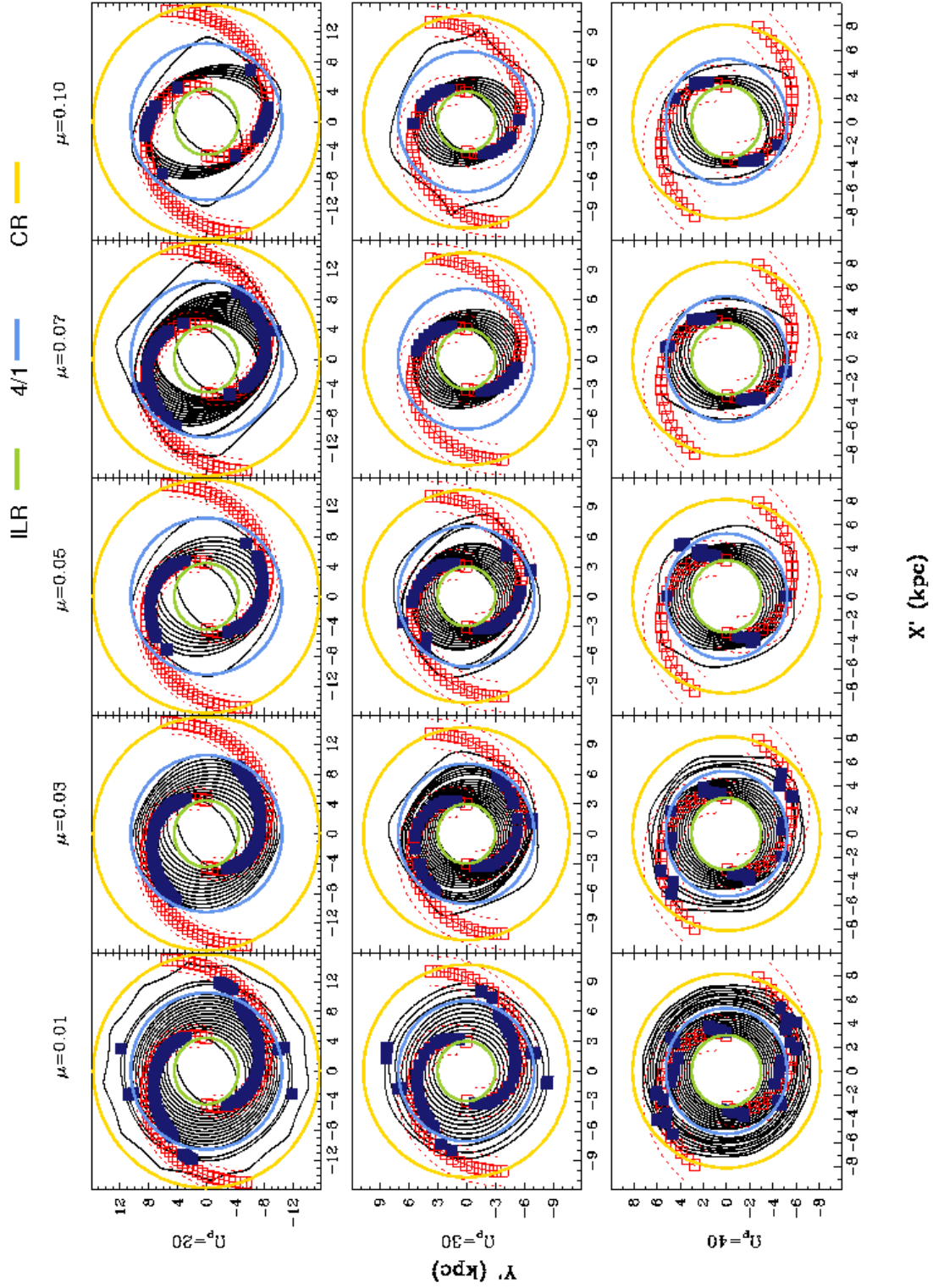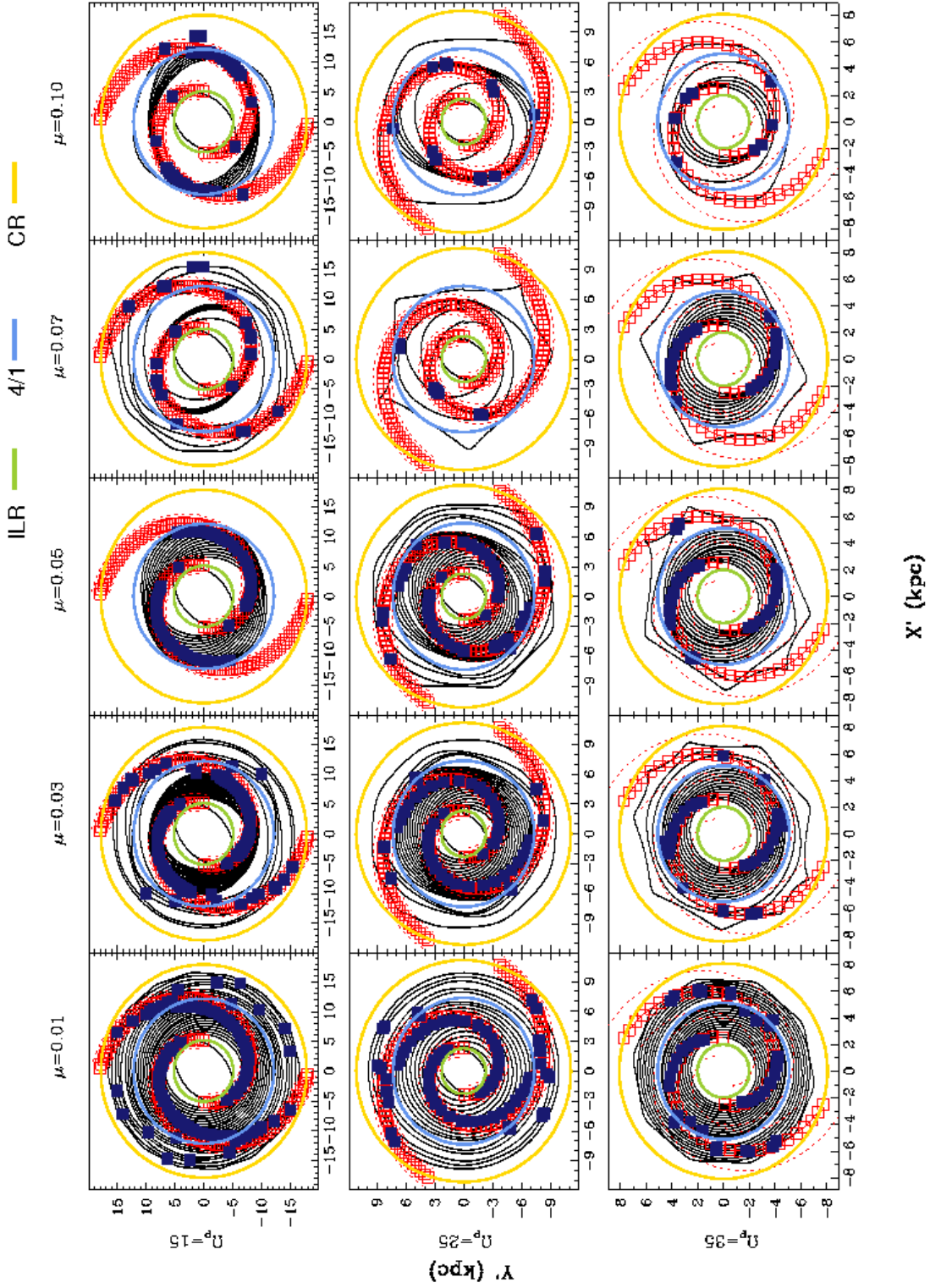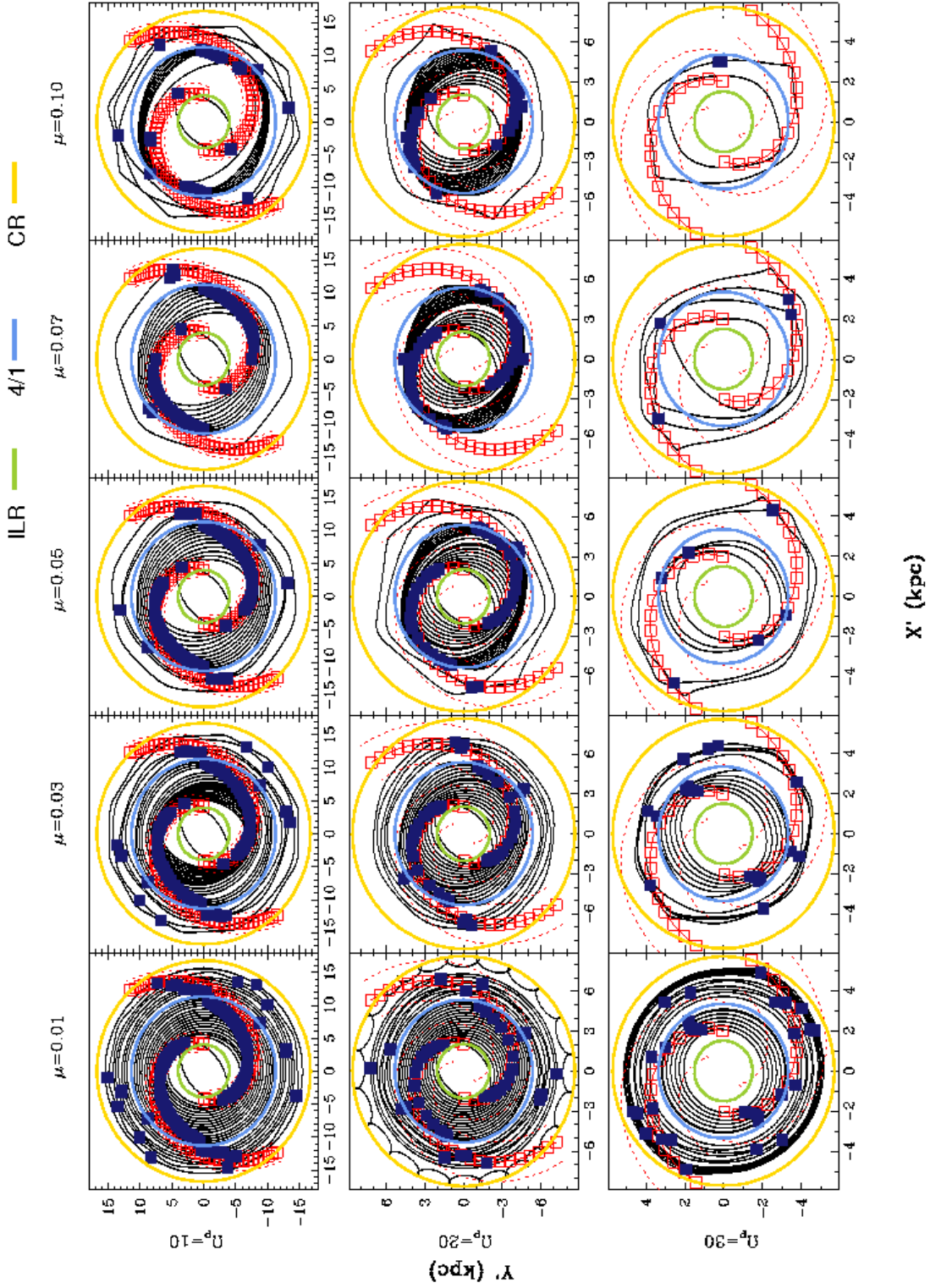
Fig. 3.— As in Figure 2, here with $i = 20°$.

Fig. 4.— Periodic orbits (black curves), density response maxima (filled squares), and the imposed spiral arms locus (open squares and dotted lines mark the width of spiral arms) for the three-dimensional spiral arms model of an Sb galaxy with a pitch angle $i = 15°$. The values of μ and $\Omega_{\rm p}$ are given at the top and left, respectively.
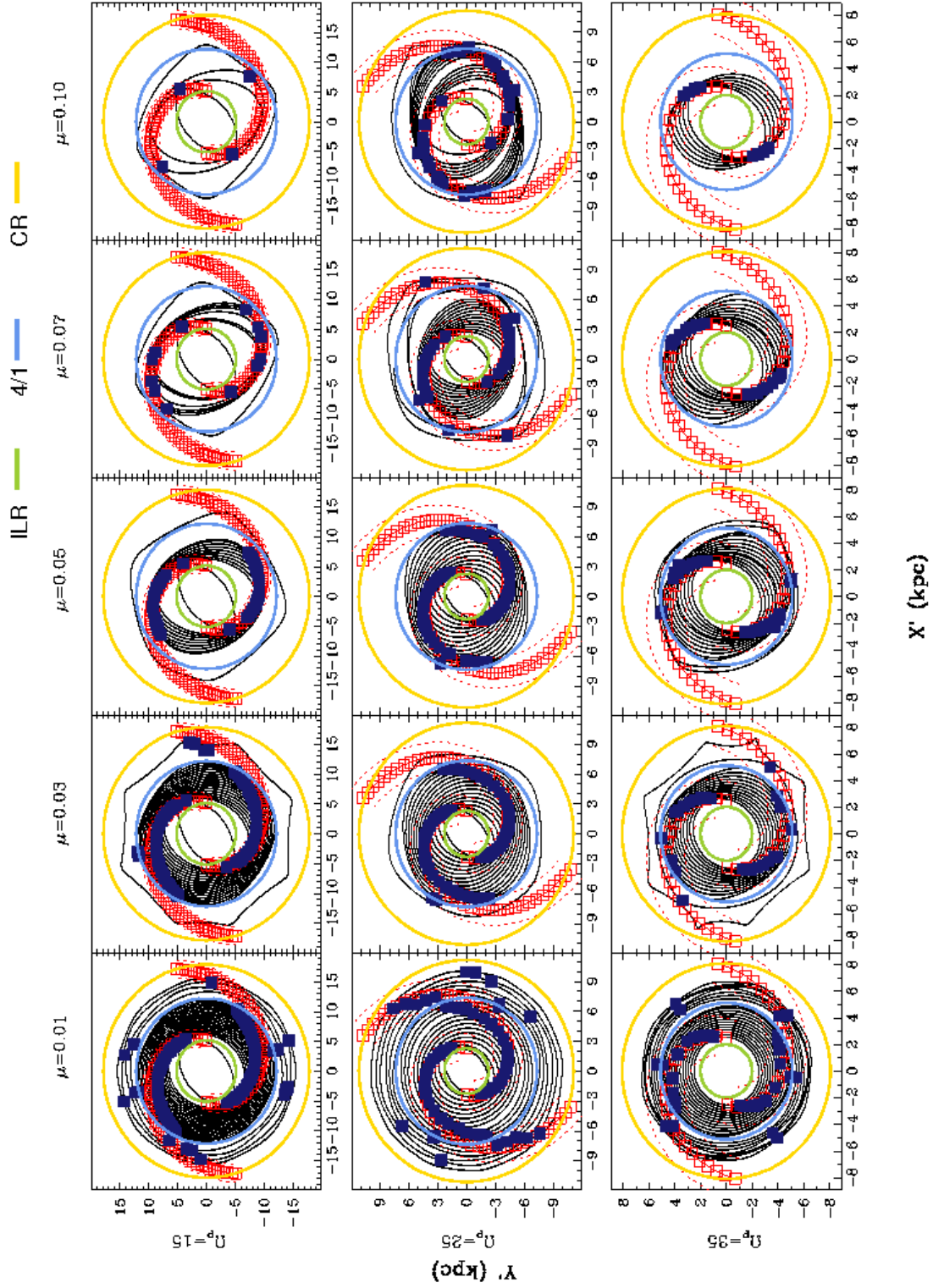
Fig. 5.— As in Figure 4, here with $i = 20°$.

Fig. 6.— Periodic orbits (black curves), density response maxima (filled squares), and the imposed spiral arms locus (open squares and dotted lines mark the width of spiral arms) for the three-dimensional spiral arms model of an Sc galaxy with a pitch angle $i = 20°$. The values of μ and $\Omega_{\rm p}$ are given at the top and left, respectively.
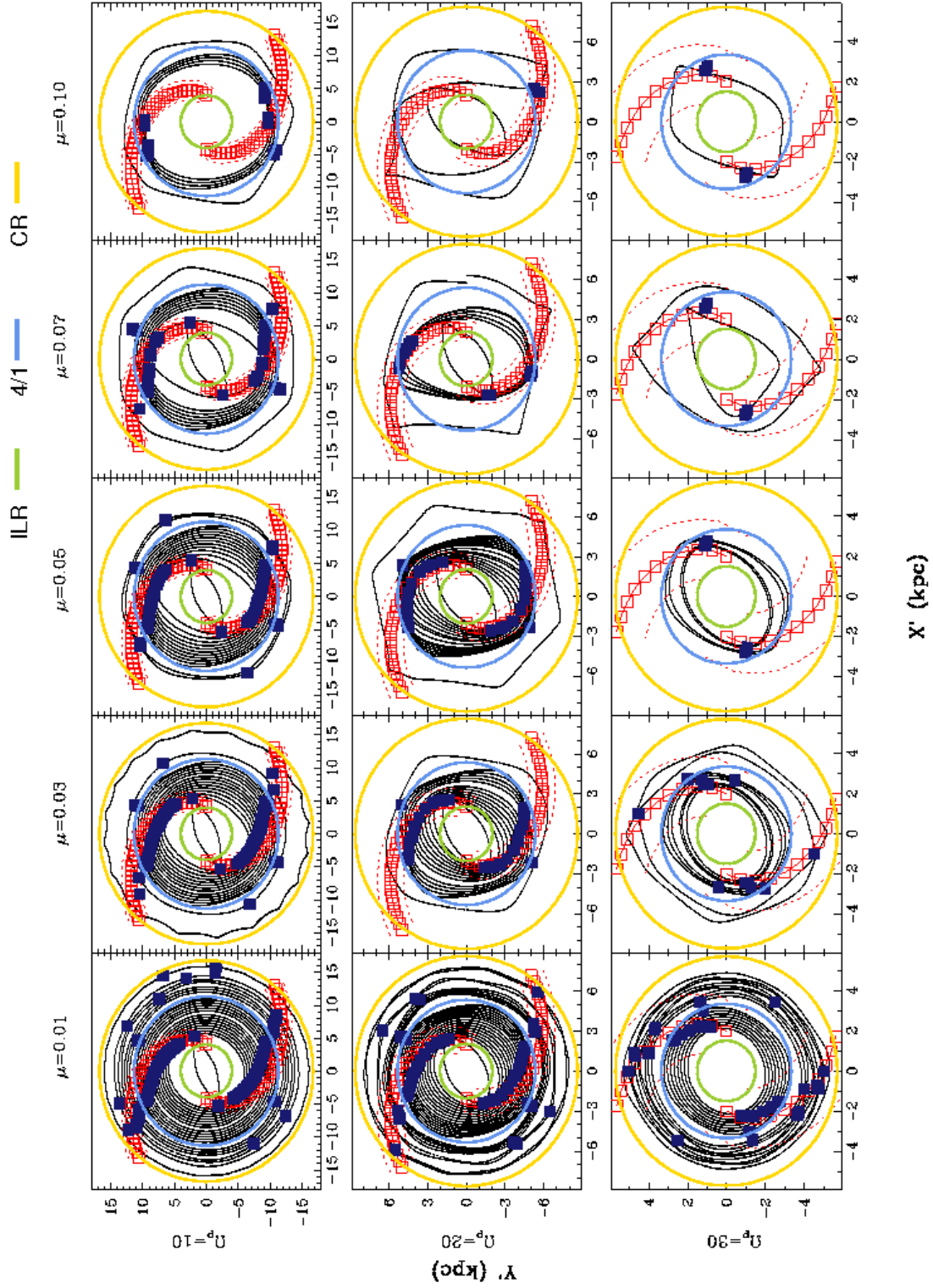
Fig. 7.— As in Figure 6, here with $i = 30°$.
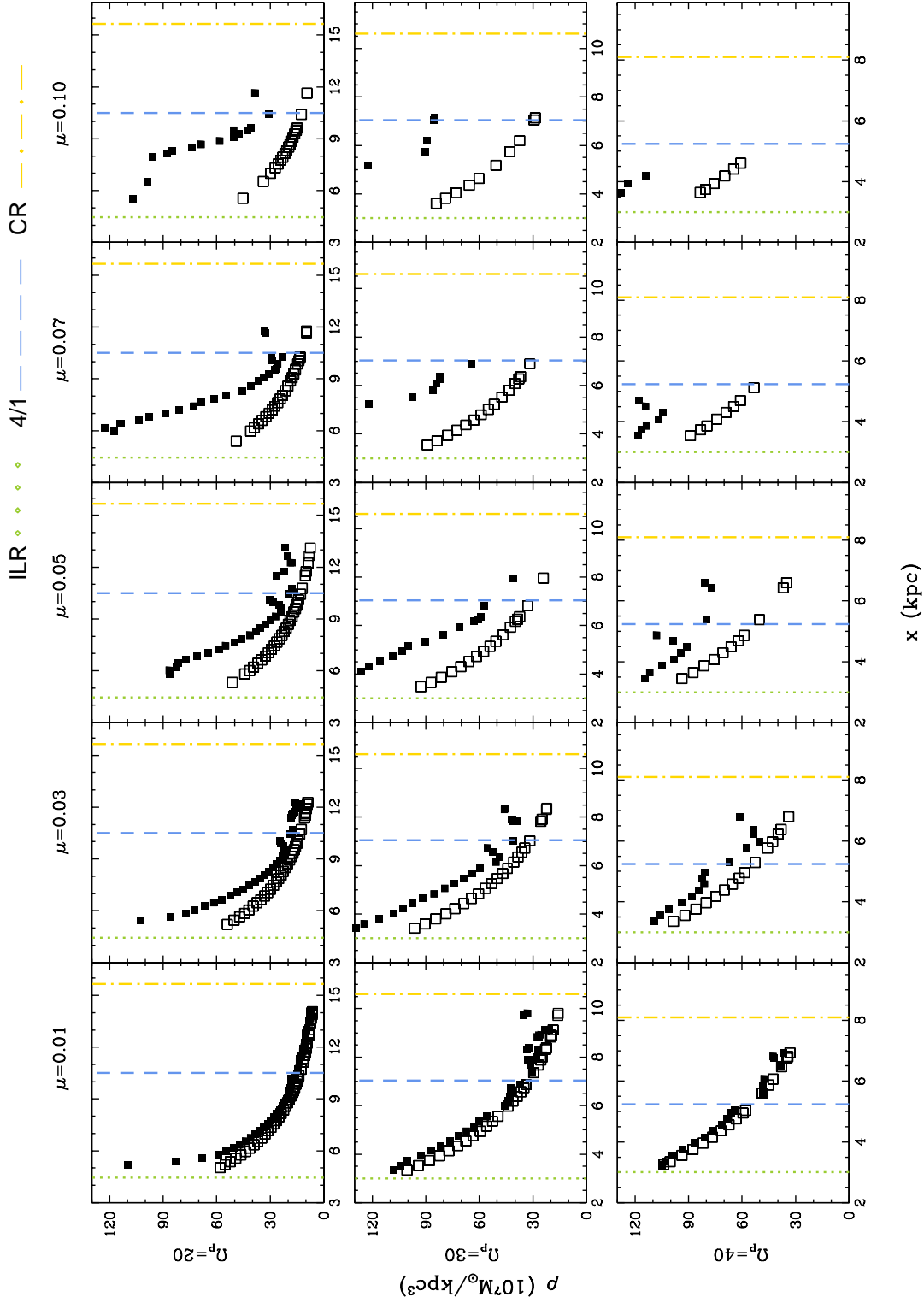
Fig. 8.— Filled squares are the density response of spiral arms for an Sa galaxy, and open squares represent the imposed density with a pitch angle $i = 10°$. The values of μ and $\Omega_{\rm p}$ are given at the top and left, respectively. The dotted, dashed and dot-dashed lines show the ILR position, 4/1 resonance position and CR position, respectively.
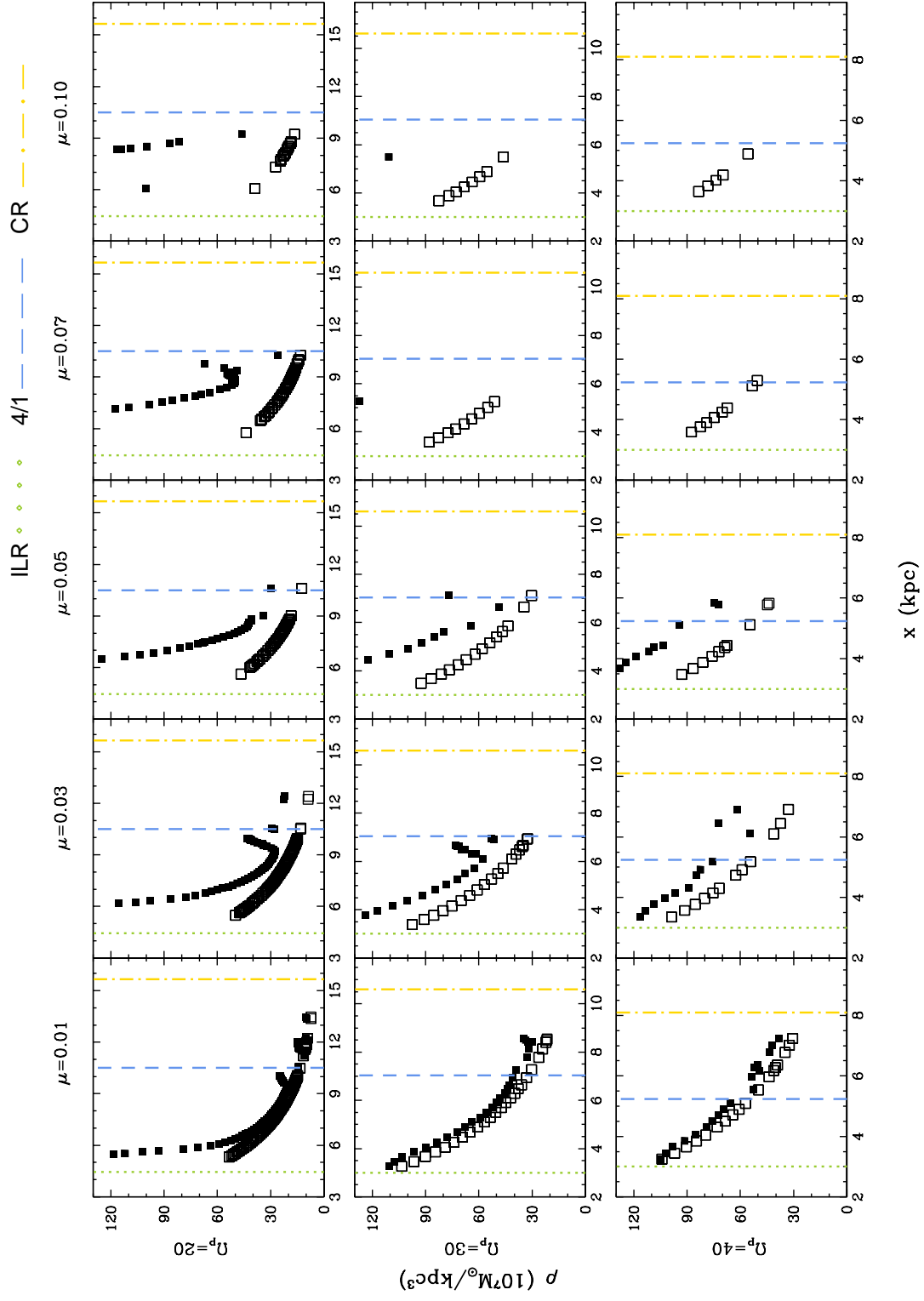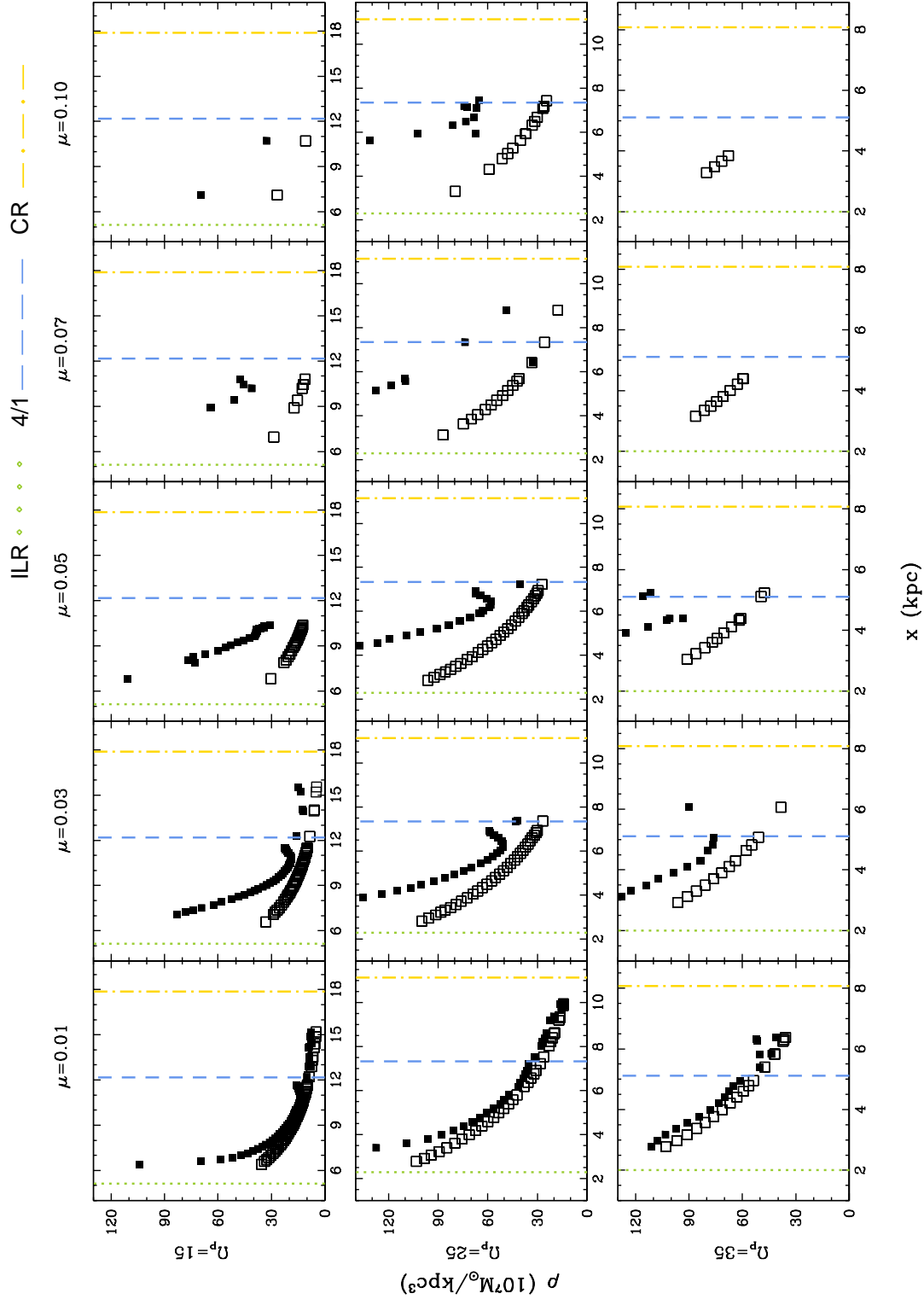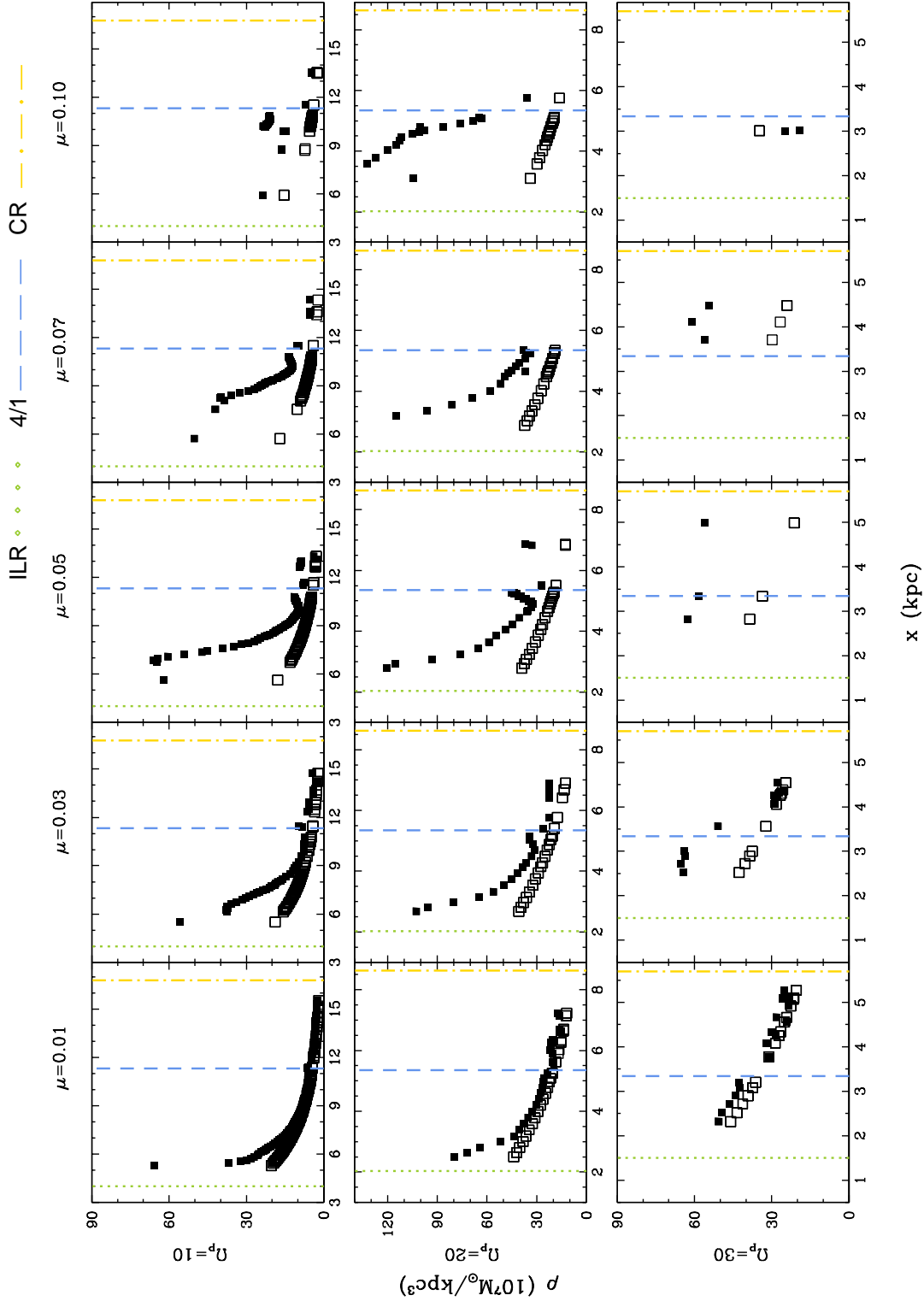
Fig. 9.— As in Figure 8, here with $i = 20°$.
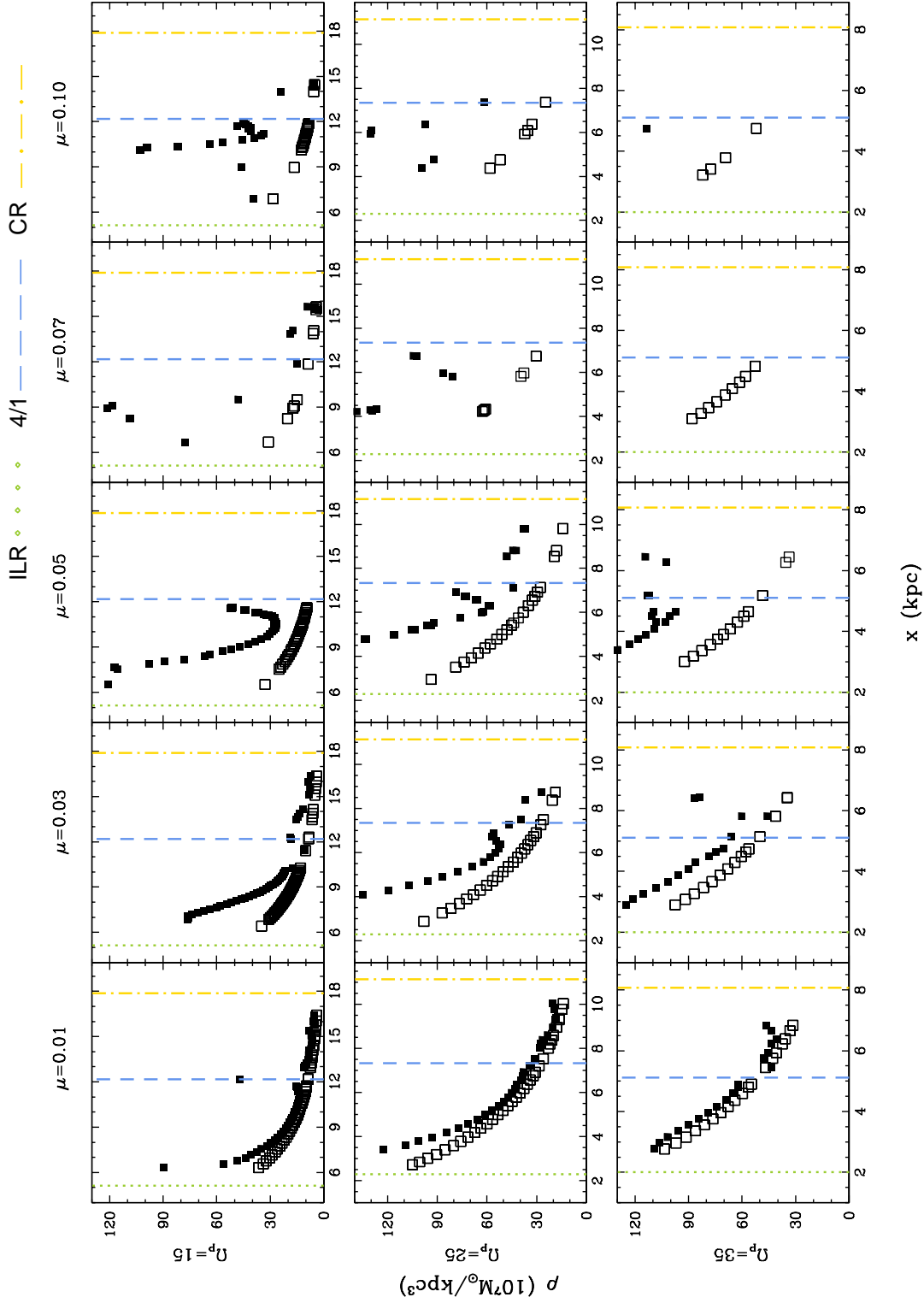
Fig. 10.— Density response diagrams. Filled squares are the density response of spiral arms for an Sb galaxy, and open squares represent the imposed density with a pitch angle $i = 15°$. The values of μ and Ω_p are given at the top and left, respectively. The dotted, dashed and dot-dashed lines show the ILR position, 4/1 resonance position and CR position, respectively.
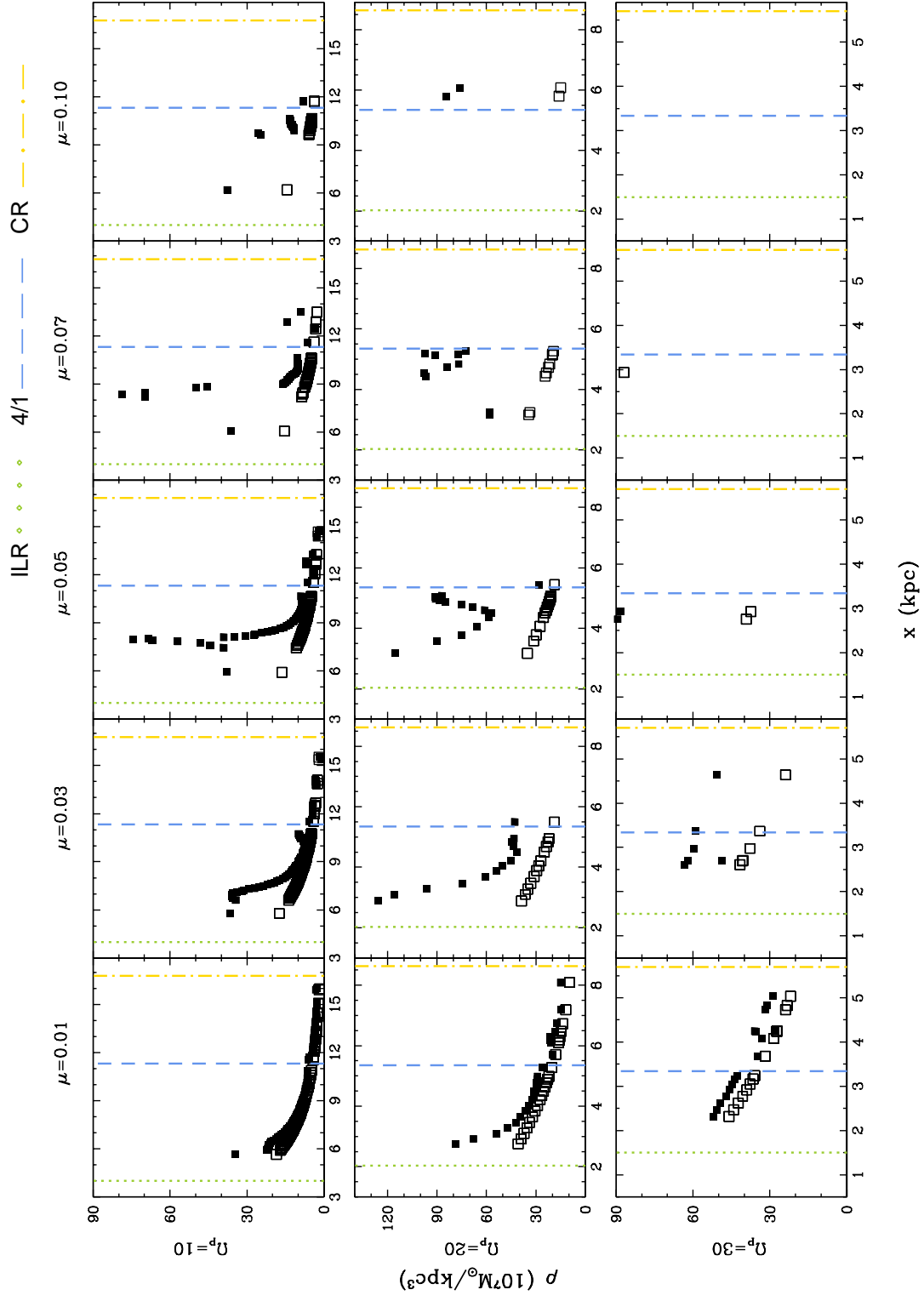
Fig. 11.— As in Figure 10, here with $i = 20°$.

Fig. 12.— Density response diagrams. Filled squares are the density response of spiral arms for an Sc galaxy, and open squares represent the imposed density with a pitch angle $i = 20°$. The values of μ and Ω_p are given at the top and left, respectively. The dotted, dashed and dot-dashed lines show the ILR position, 4/1 resonance position and CR position, respectively.

Fig. 13.— As in Figure 12, here with $i = 30°$.

outer galaxy, even in some cases passing the corotation barrier. In the Poincaré diagrams we varied the spiral arms mass, and their angular velocity and pitch angle, as we did with the periodic orbital study. The analysis of the chaotic behavior is relevant because it can provide constraints to the maximum values of some important parameters of galaxies (pitch angle or spiral arms masses, for example). With this study, we find a limit to the spiral arms mass, for which chaos becomes pervasive dominating the available phase space and destroying all periodic orbits as well as the ordered orbits surrounding them.

We present a set of Poincaré diagrams for each morphological type. In our experiments, assorted spiral arms masses, pitch angles and angular velocities are tested. We explored a comprehensive set of E_J families, from energies representing the most bounded orbits (galactic centers) to the corotation barrier and beyond to cover the total extension of the spiral arms. The values presented in the mosaics of Poincaré diagrams correspond approximately to the CR position in each case (that represent the most extreme and clear cases, regarding chaos). For energies more bounded the presence of chaos diminishes, but the general behavior is similar, i.e., if the pitch angle (or mass) increases chaos increases in the different energies. However, when chaos becomes pervasive and the main periodic orbits are destroyed, the chaotic behavior dominates in bounded energies as much as closer to corotation.

Figures 14 to 19 show phase-space diagrams for Sa, Sb, and Sc galaxies, considering in each type two values of the pitch angle. The common trend in all these diagrams is that the chaotic region which appears in the prograde (left) sides increases as μ and $\Omega_{\rm p}$ increase. This chaotic region extends toward the inner galactic region, destroying periodic orbits that could support the spiral arms. In each galactic type the chaotic region is more extended for the larger employed value of i, and it is also markedly stronger for an Sc galaxy.

In summary, analyzing orbital self-consistency through periodic orbits, we find that in order to produce long-lasting spiral arms, the ratio μ in early spiral galaxies can be much larger than in late spiral galaxies without compromising the stability of the arms. Consequently, when the pitch angle is smaller, the limit for μ can be considerably larger. Approximately, the intervals in i and μ to obtain long-lasting spiral arms in this scheme are the following: for an Sa galaxy with $\Omega_{\rm p} \sim 30\,{\rm km\,s^{-1}\,kpc^{-1}}$, $i \lesssim 10°$ and $\mu \lesssim 0.07$; for an Sb galaxy with $\Omega_{\rm p} \sim 25\,{\rm km\,s^{-1}\,kpc^{-1}}$, $i \lesssim 15°$ and $\mu \lesssim 0.05$; and for an Sc galaxy with $\Omega_{\rm p} \sim 20\,{\rm km\,s^{-1}\,kpc^{-1}}$, $i \lesssim 20°$ and $\mu \lesssim 0.03$. For greater values than these, the spiral arms would be rather explained as transient structures. The limits for μ are only examples that depend on the values of i and $\Omega_{\rm p}$; this means that these parameters are deeply interrelated.

Regarding the chaotic behavior, with phase-space studies we also found a maximum value for μ, before chaos becomes pervasive destroying the main periodic orbits which give support to spiral arms. As we mentioned in the ordered case, the maximum limit of μ is mainly linked to i and less to $\Omega_{\rm p}$. Therefore, when i is smaller, the limit for μ can be larger, this is due to both parameters are related to the spiral arm force (or amplitude of the force). An example of the limits for μ
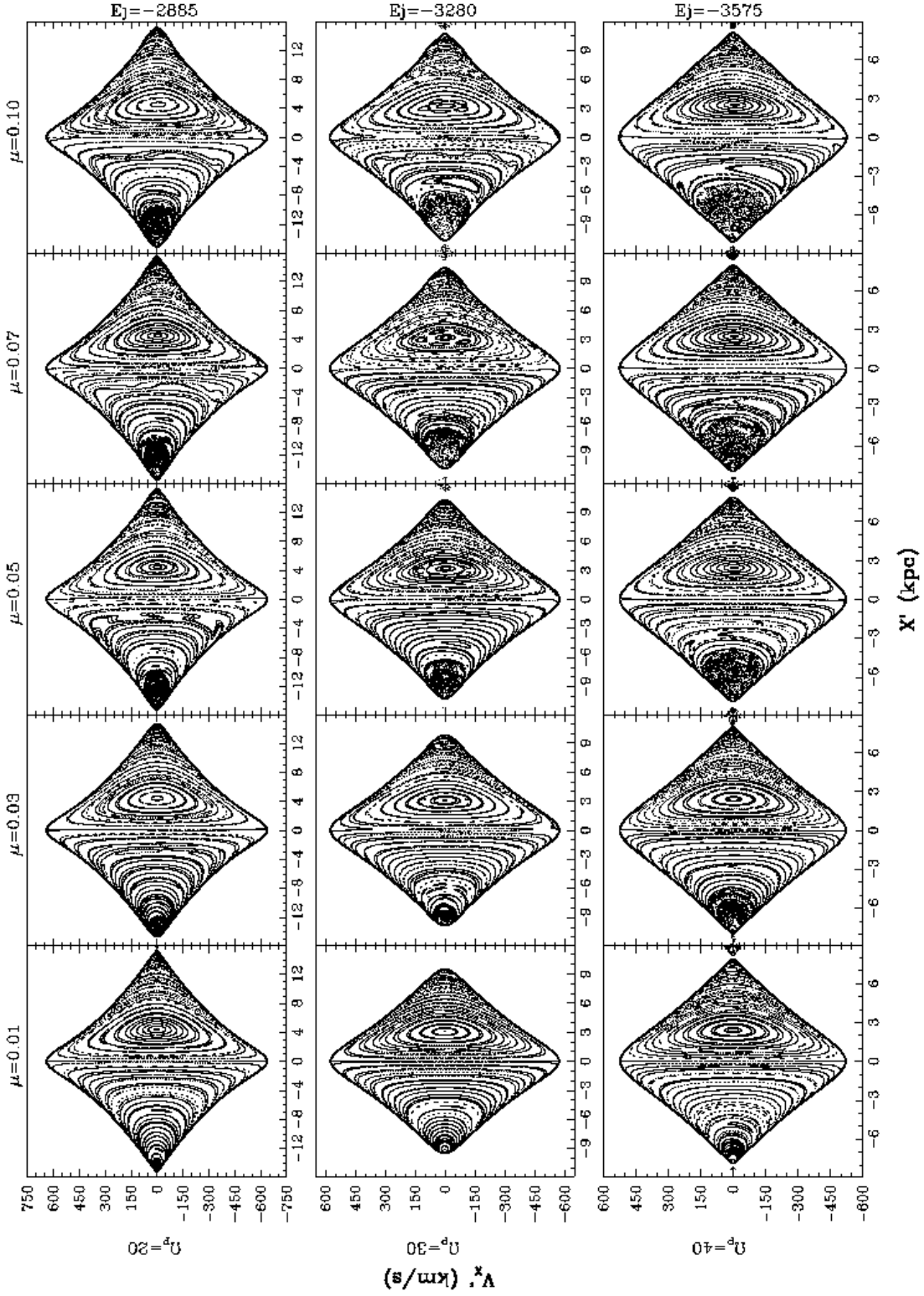
Fig. 14.— Phase-space diagrams for an Sa galaxy with $i = 10°$. The values of the Jacobi energy, μ, and Ω_{p}, are given at the right, top, and left, respectively.
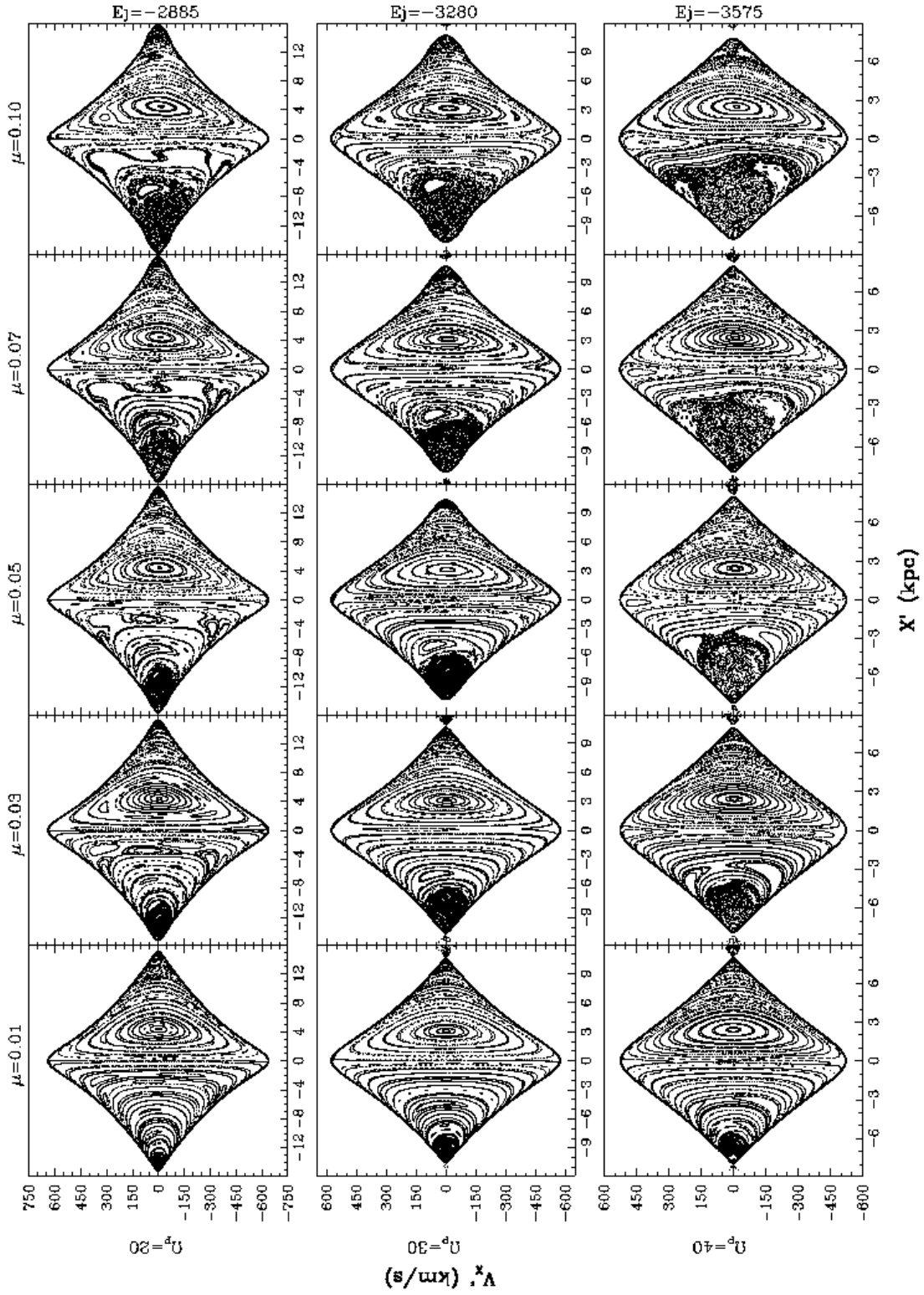
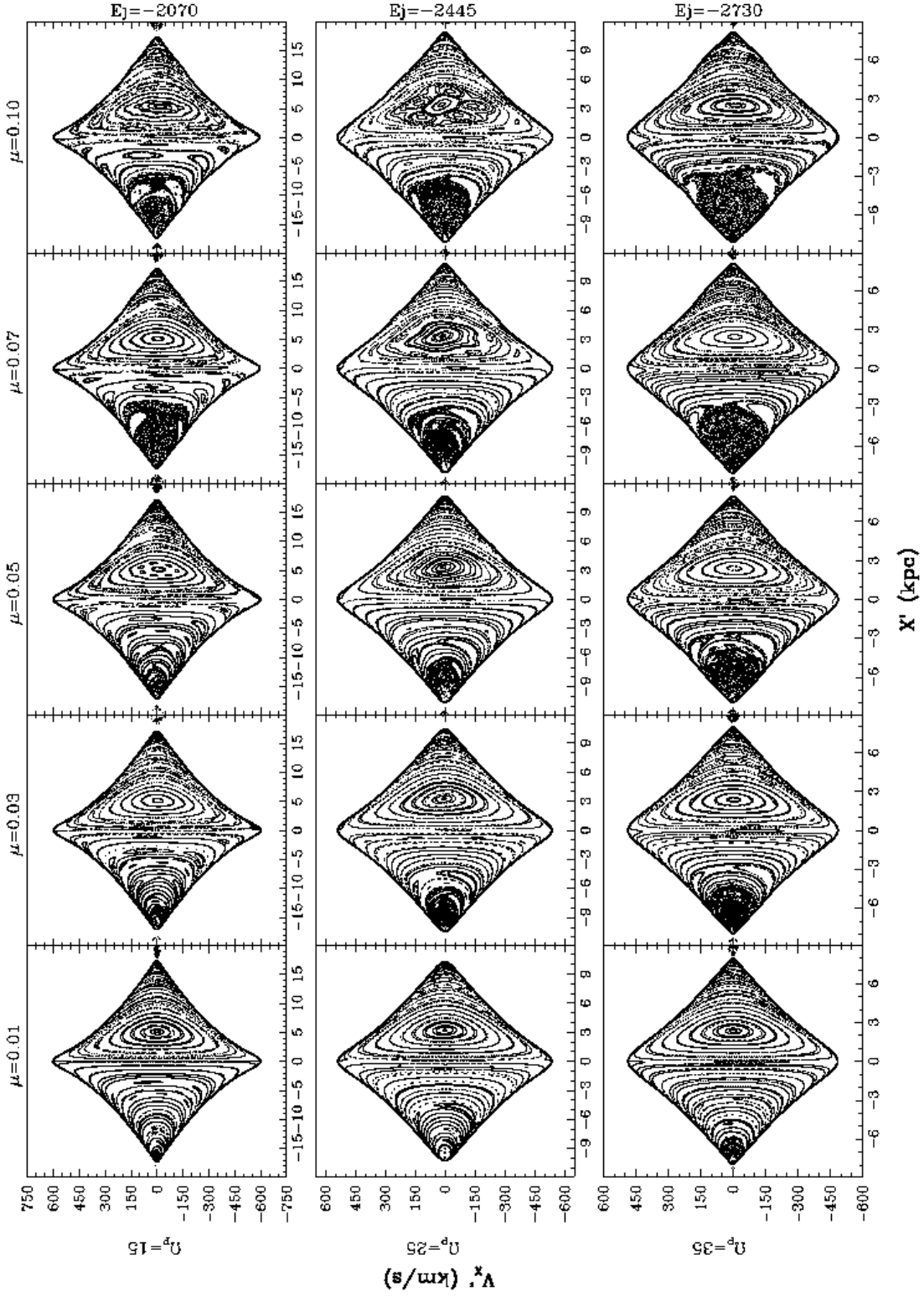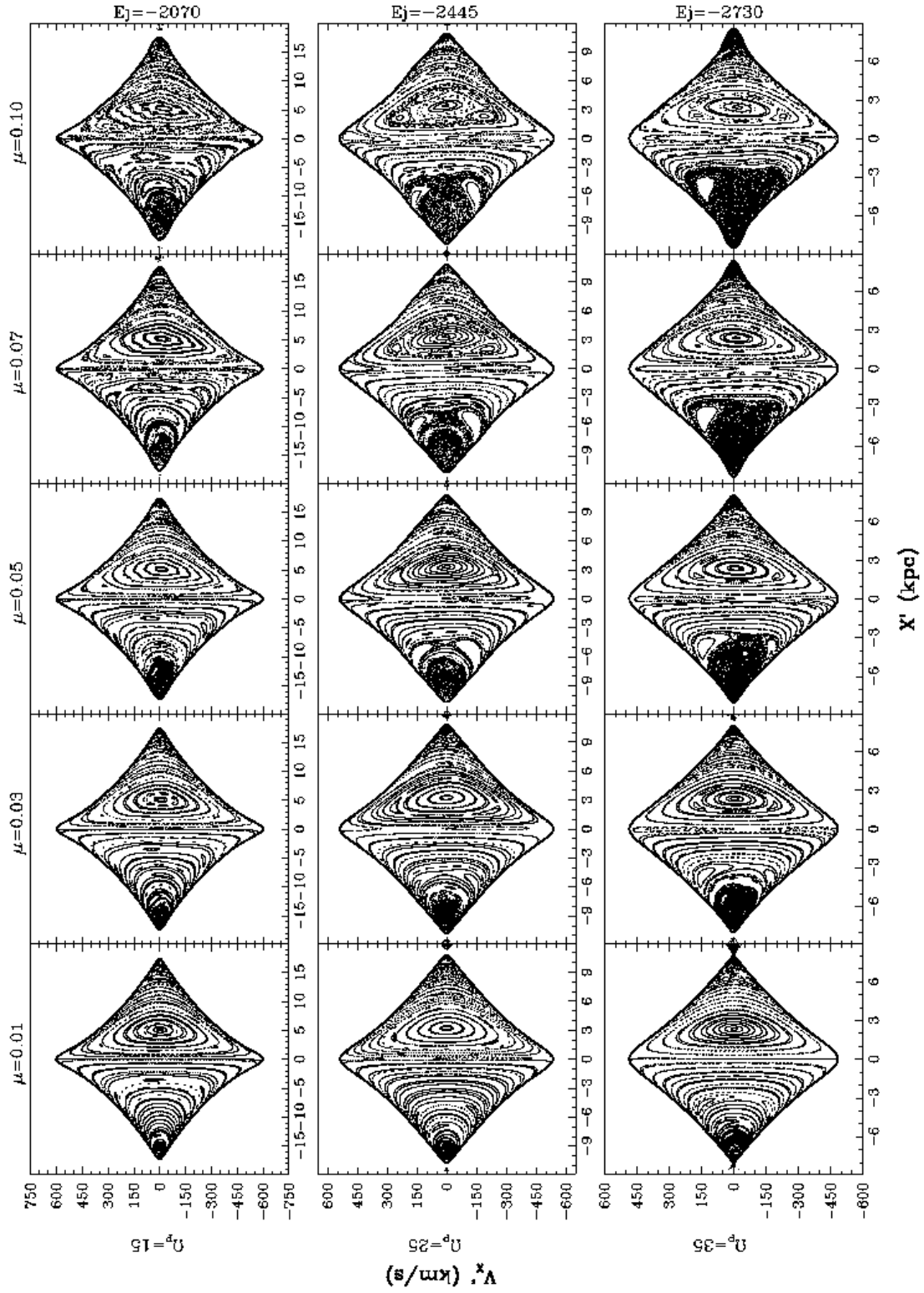Fig. 15.— As in Figure 14, here with $i = 20°$.

Fig. 16.— Phase-space diagrams for an Sb galaxy with $i = 15°$. The values of the Jacobi energy, μ, and Ω_p, are given at the right, top, and left, respectively.

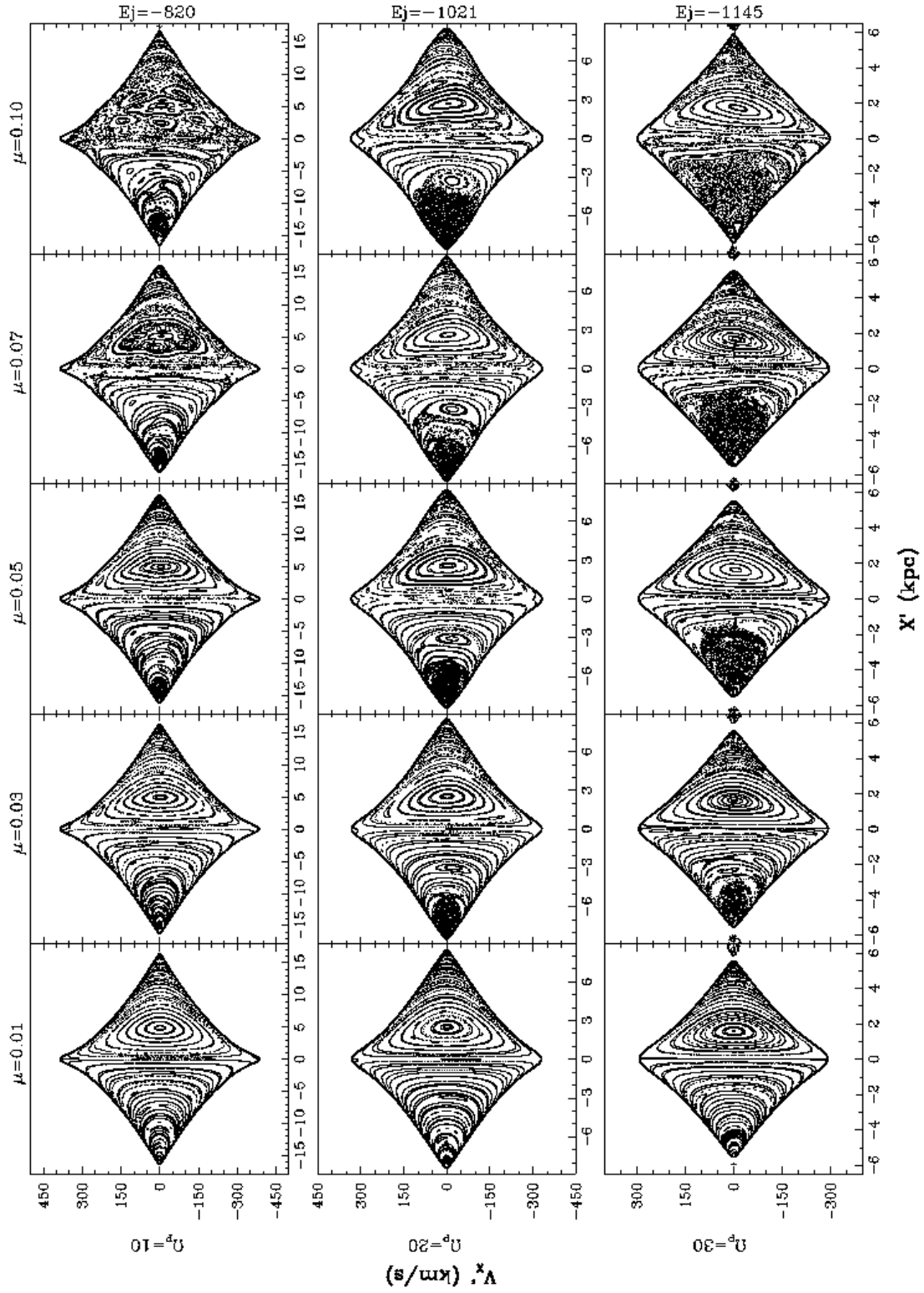Fig. 17.— As in Figure 16, here with $i = 20°$.

Fig. 18.— Phase-space diagrams for an Sc galaxy with $i = 20°$. The values of the Jacobi energy, μ, and $\Omega_{\rm p}$, are given at the right, top, and left, respectively.
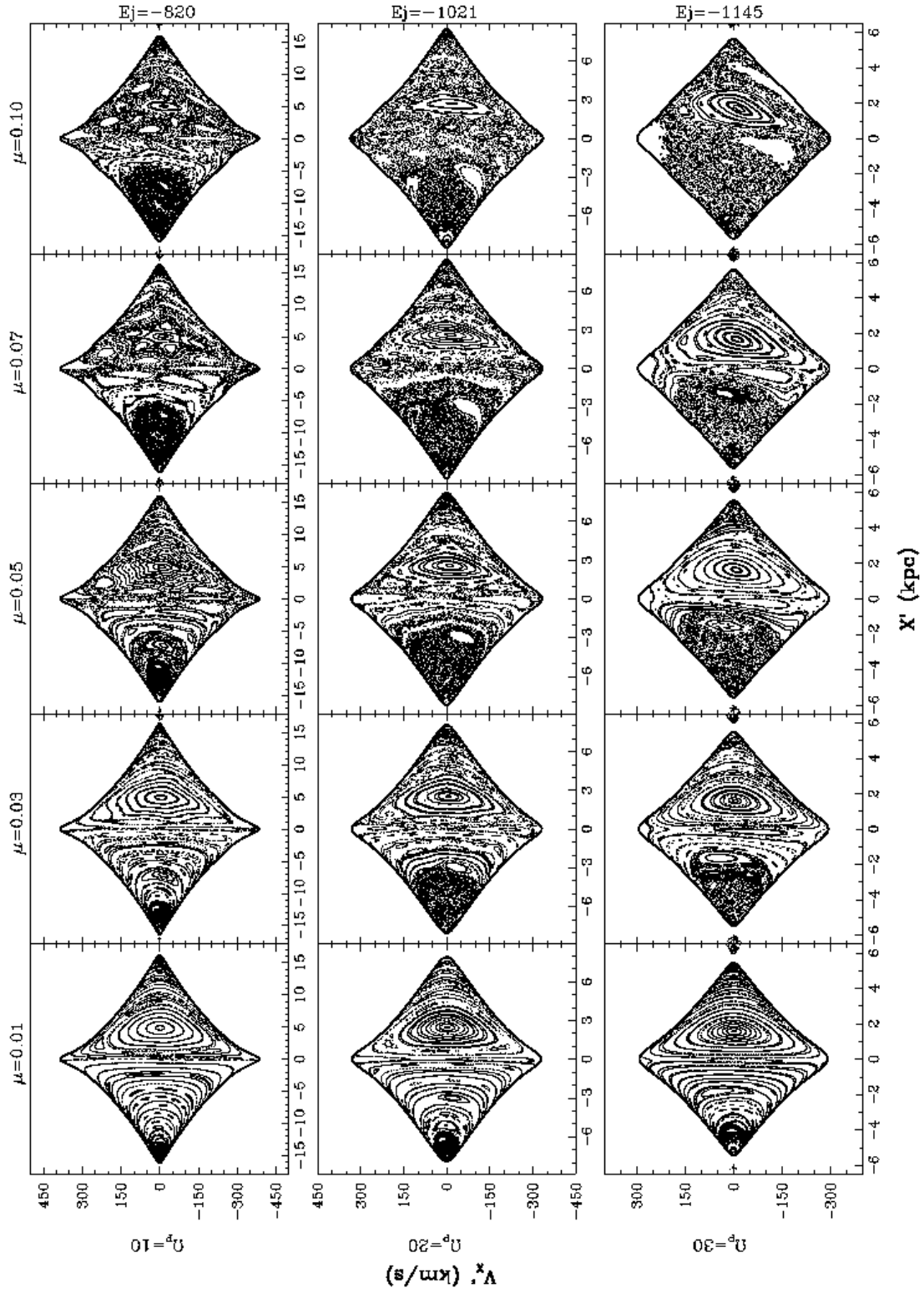
Fig. 19.— As in Figure 18, here with $i = 30°$.

depending on i and Ω_p are: for an Sa galaxy, $\mu \lesssim 0.1$, with $i \lesssim 20°$ and $\Omega_p \sim 40 \, \mathrm{km \, s^{-1} \, kpc^{-1}}$; for an Sb galaxy, $\mu \lesssim 0.07$, with $i \lesssim 20°$ and $\Omega_p \sim 35 \, \mathrm{km \, s^{-1} \, kpc^{-1}}$; and for an Sc galaxy, $\mu \lesssim 0.05$, with $i \lesssim 30°$ and $\Omega_p \sim 20 \, \mathrm{km \, s^{-1} \, kpc^{-1}}$. For grater values of μ the spiral arms are destroyed by chaotic behavior.

This analysis are some selected examples to clarify the general orbital behavior. In Section 4 we will summarize in a set of plots the ordered and chaotic behavior, taking a significant increase in the number of values of the parameters μ and i employed.

3.2. Orbital Study Analyzing the Effect of the Angular Velocity of the Spiral Arms: Ordered and Chaotic Behavior

In Section 3.1, we have analyzed the effect of the mass of the spiral arms on the ordered and chaotic stellar dynamics on the equatorial plane of normal spiral galaxies; for this purpose we employed assorted masses, pitch angles and angular velocities of the spiral arms. In this Section we present a similar orbital study, analyzing the effect in the ordered and chaotic stellar dynamics as we vary Ω_p in an extended interval, from 10 to 60 $\mathrm{km \, s^{-1} \, kpc^{-1}}$ for each morphological type. As in the case of the spiral-arms-mass analysis, in order to dilucidate their relative importance, we also slightly change other parameters; for the pitch angle we take respectively the values 7°, 18°, and 25°, in Sa, Sb, Sc galactic types, and in all these galactic types μ takes the values 0.01, 0.03, and 0.05. As in the previous subsection, these are only some examples to obtain a perception of the dynamical behavior exerted by changes in the spiral arms parameters. In the next section we summarize the results.

In Figure 20 we present periodic orbits for an Sa galaxy with $i = 7°$. This figure shows that the amount of periodic orbits which give support to the spiral arms decrease with Ω_p and μ. For $\Omega_p \lesssim 30 \, \mathrm{km \, s^{-1} \, kpc^{-1}}$, the density response follows the imposed spiral arms potential almost to the CR position; for $\Omega_p \sim 40 \, \mathrm{km \, s^{-1} \, kpc^{-1}}$, the density support extends slightly beyond the 4/1 resonance position. This behavior is obtained with $\mu \sim 0.01$. If μ increases between 0.03 and 0.05 the density support extends beyond the 4/1 resonance position. For $\Omega_p > 40 \, \mathrm{km \, s^{-1} \, kpc^{-1}}$, there is no density support. If we increase the pitch angle to 18°, the density support extends almost to the CR position only if $\mu \lesssim 0.01$; above this value of μ there is a density support up to the 4/1 resonance. If $\Omega_p > 30 \, \mathrm{km \, s^{-1} \, kpc^{-1}}$ and $\mu \lesssim 0.05$, the density support reaches the 4/1 resonance position. Thus, the orbital support depends on three parameters of the spiral arms: their pitch angle, mass, and angular speed, being the dependence on the first parameter, the more sensitive. The value of this parameter is the one with the wider possible range in galaxies.

Figure 21 shows periodic orbits for an Sb galaxy with $i = 18°$. For $\Omega_p \lesssim 30 \, \mathrm{km \, s^{-1} \, kpc^{-1}}$ and $\mu = 0.01$, the density support extends approximately up to the CR position. For $\Omega_p = 40 \, \mathrm{km \, s^{-1} \, kpc^{-1}}$ and $\mu = 0.01$ this support extends only up to the 4/1 resonance. If $\mu > 0.01$ the density support extends up to the 4/1 resonance but producing a pitch angle smaller than in the
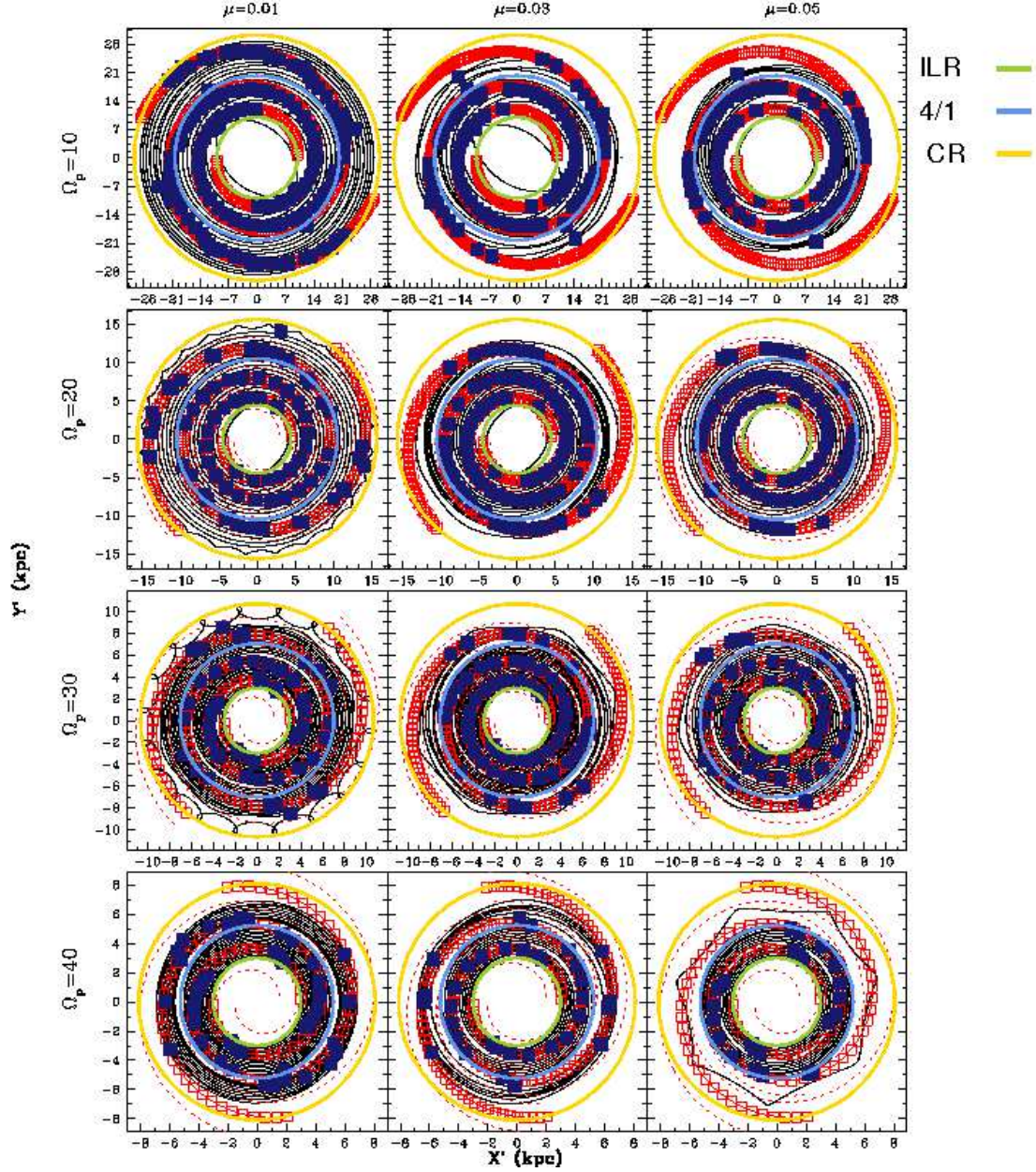
Fig. 20.— Periodic orbits (black curves), density response maxima (filled squares), and the imposed spiral arms locus (open squares and dotted lines mark the width of spiral arms) for the three-dimensional spiral arms model of an Sa galaxy with a pitch angle $i = 7°$. The values of μ and Ω_p are given at the top and left, respectively.

imposed arms. For cases where $\Omega_{\rm p} > 40\,{\rm km\,s^{-1}\,kpc^{-1}}$, there is no density support.

In Figure 22 we show periodic orbits for an Sc galaxy with $i = 25°$. For $\Omega_{\rm p} \lesssim 30$ and $\mu = 0.01$, the density support extends not far from the CR position. For $\mu = 0.03$, 0.05, this support extends up to the 4/1 resonance position (in some cases slightly beyond) forming a smaller pitch angle than in the imposed arms. With $\mu = 0.05$ there is no density support if $\Omega_{\rm p} \sim 30\,{\rm km\,s^{-1}\,kpc^{-1}}$ or larger.

As we did in the case where we analyzed the effect of spiral arms mass, we have compared the spiral arms density response (filled squares) with the spiral arms imposed density (PERLAS, open squares). We constructed a mosaic of density response corresponding to each periodic orbit mosaic. Figures 23, 24 and 25 show the densities for Sa, Sb and Sc galaxies, respectively. With these mosaics we reinforce the results presented with periodic orbits and maxima density response in Figures 20 - 22.

Now, in order to analyze the chaotic behavior, as was done varying the mass of spiral arms (Section 3.1), in this part we also present a detailed study of Poincaré diagrams varying the angular speed of the spiral arms in an extended interval. We change slightly the mass of the spiral arms and the pitch angle. With this analysis we found a limit to the angular speed for which chaos becomes pervasive, dominating the available phase space and destroying all the periodic orbits as well as the ordered orbits surrounding them.

Figure 26 shows Poincaré diagrams for an Sa galaxy with $i = 7°$. For $\Omega_{\rm p} = 10$ and $20\,{\rm km\,s^{-1}\,kpc^{-1}}$ the orbital behavior is ordered; however the chaotic regions emerge when μ increases from 0.01 to 0.05. For $\Omega_{\rm p} = 30$ and $40\,{\rm km\,s^{-1}\,kpc^{-1}}$, the ordered orbits dominate, but even with $\mu = 0.01$ the chaotic behavior already appears in the prograde region, and increases with μ. If $i = 15°$ the chaotic behavior increases with the mass and angular speed of the spiral arms.

Figure 27 shows Poincaré diagrams for an Sb galaxy with $i = 18°$. The ordered orbits dominate the prograde region and there is a small region of chaos, which increases slightly with $\Omega_{\rm p}$. Additionally, the orbits are more complex and resonant islands appear. A severe increment of the chaotic region towards the main periodic orbits supporting the spiral arms is related with an increment of μ; for example, when $\mu = 0.05$ and $\Omega_{\rm p} = 40\,{\rm km\,s^{-1}\,kpc^{-1}}$, the chaotic behavior covers an important part of the prograde region.

Figure 28 shows Poincaré diagrams for an Sc galaxy with $i = 25°$. The majority of orbits are ordered, but the chaotic region slowly increases with $\Omega_{\rm p}$. The chaotic behavior is more prone to emerge when μ is larger; for example, if $\mu = 0.05$ and $\Omega_{\rm p} = 40\,{\rm km\,s^{-1}\,kpc^{-1}}$ chaos dominates an important region of the available phase-space, covering practically all the prograde region and destroying the periodic orbits.

In summary, regarding ordered behavior, we constrain the angular speed of the spiral arms through the existence of periodic orbits. We found that the orbital support for these arms depends on three parameters: the pitch angle, mass, and angular speed, but the orbital support seems to be much more sensitive first to the pitch angle, and second to the mass of spiral arms, and almost
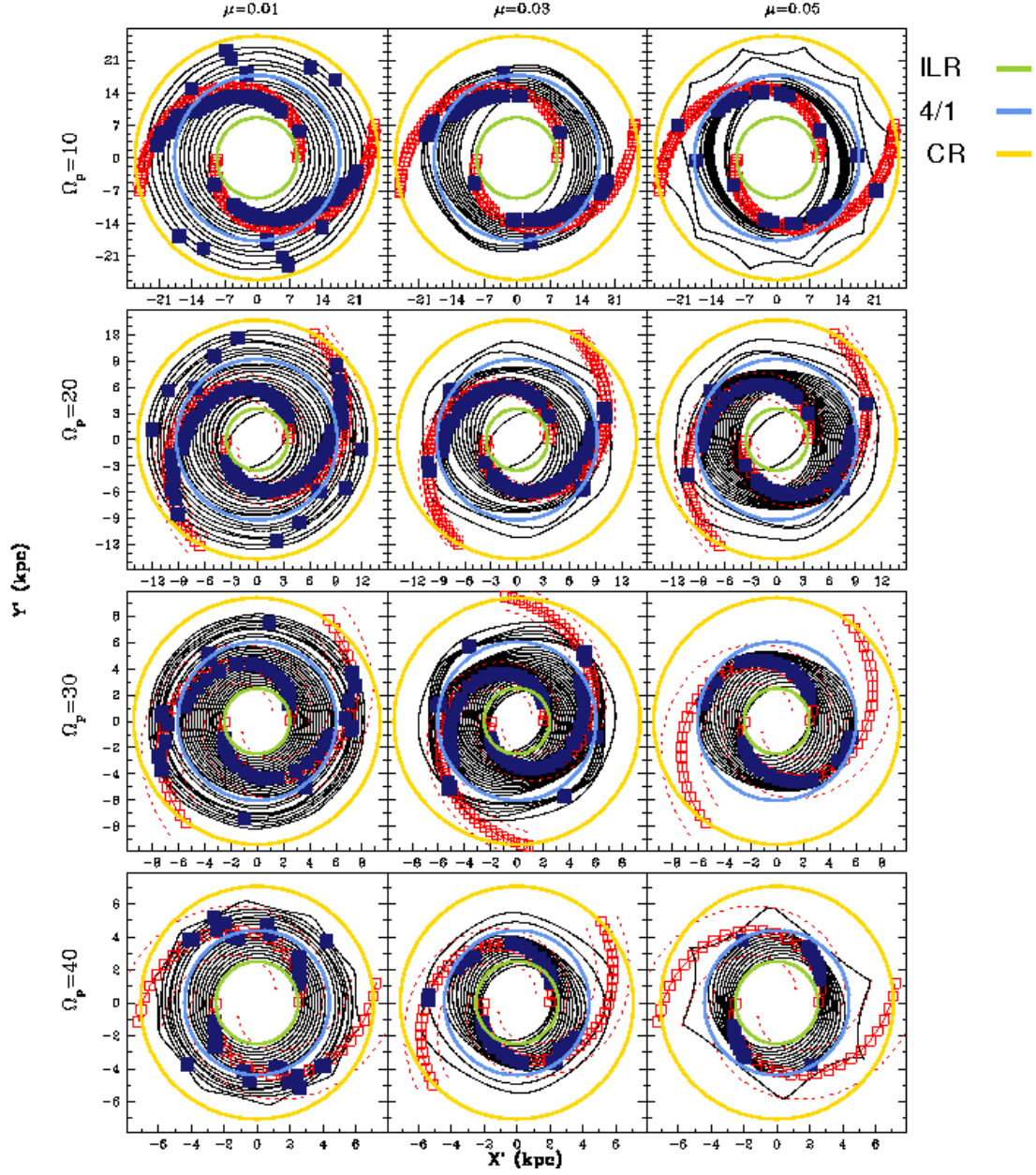
Fig. 21.— As in Figure 20, here for an Sb galaxy with $i = 18°$.

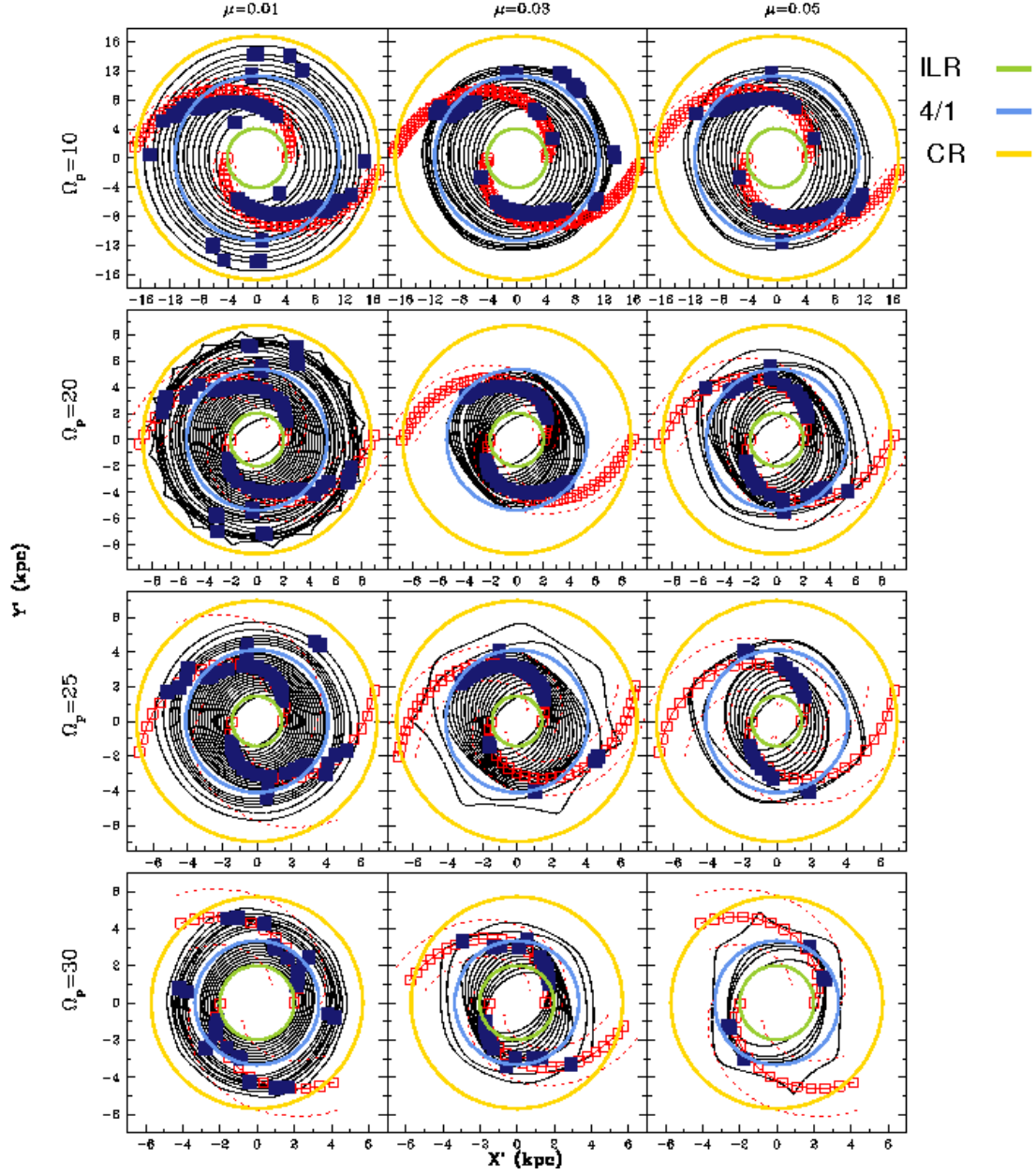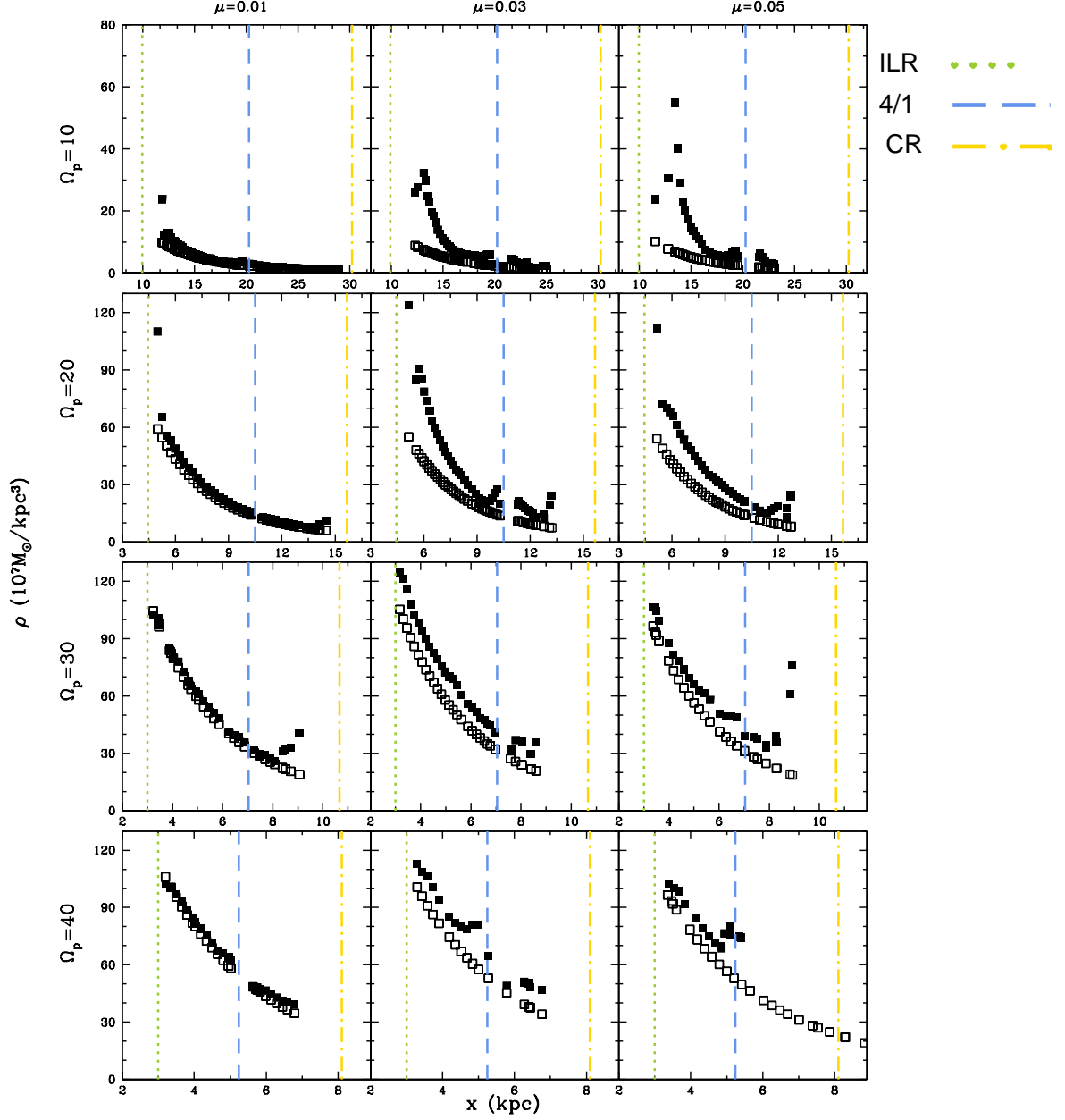Fig. 22.— As in Figure 20, here for an Sc galaxy with $i = 25°$.

Fig. 23.— Density response diagrams. Filled squares are the density response of spiral arms for an Sa galaxy, and open squares represent the imposed density with a pitch angle $i = 7°$. The values of μ and Ω_p are given at the top and left, respectively. The dotted, dashed and dot-dashed lines show the ILR position, 4/1 resonance position and CR position, respectively.
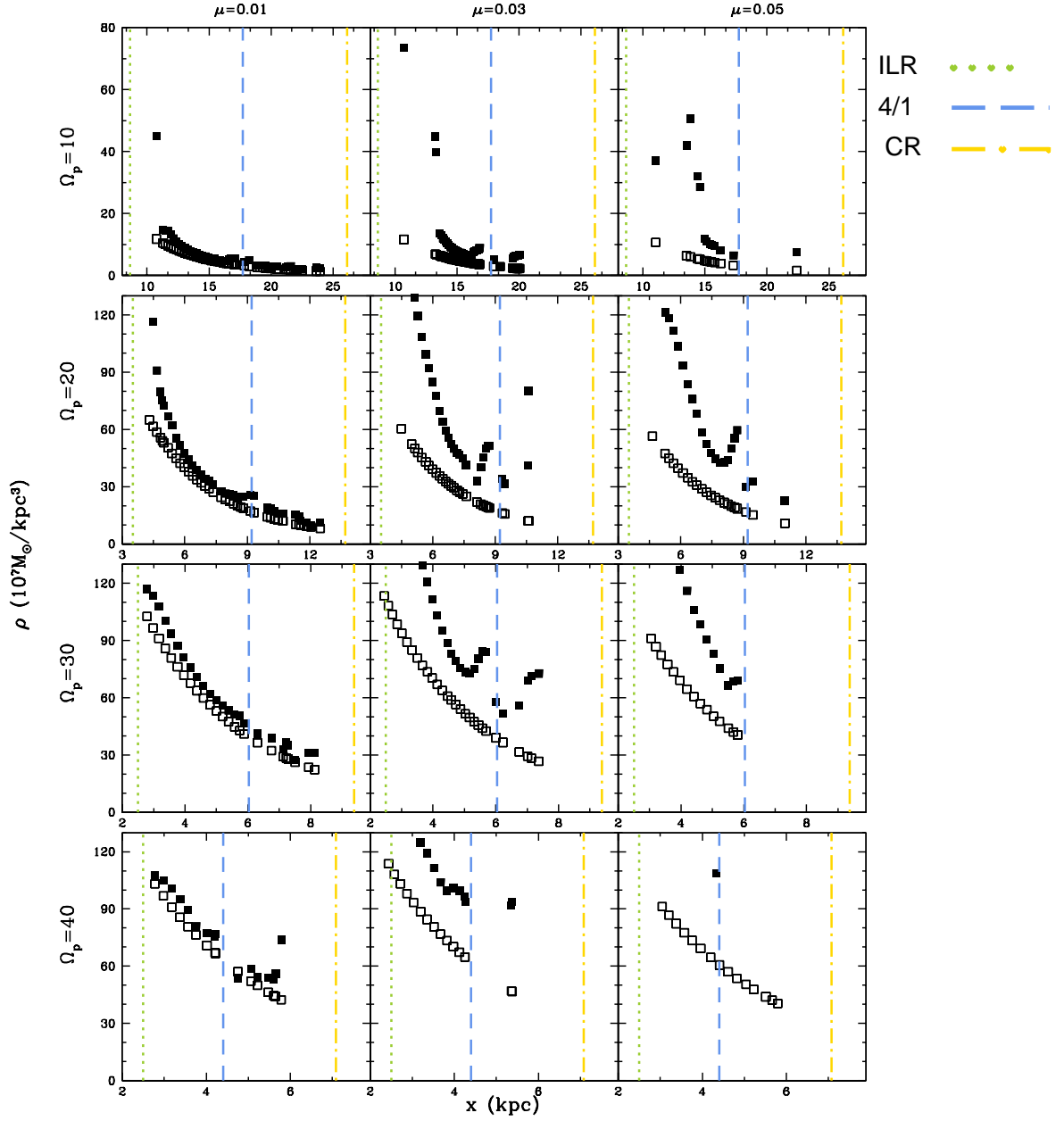
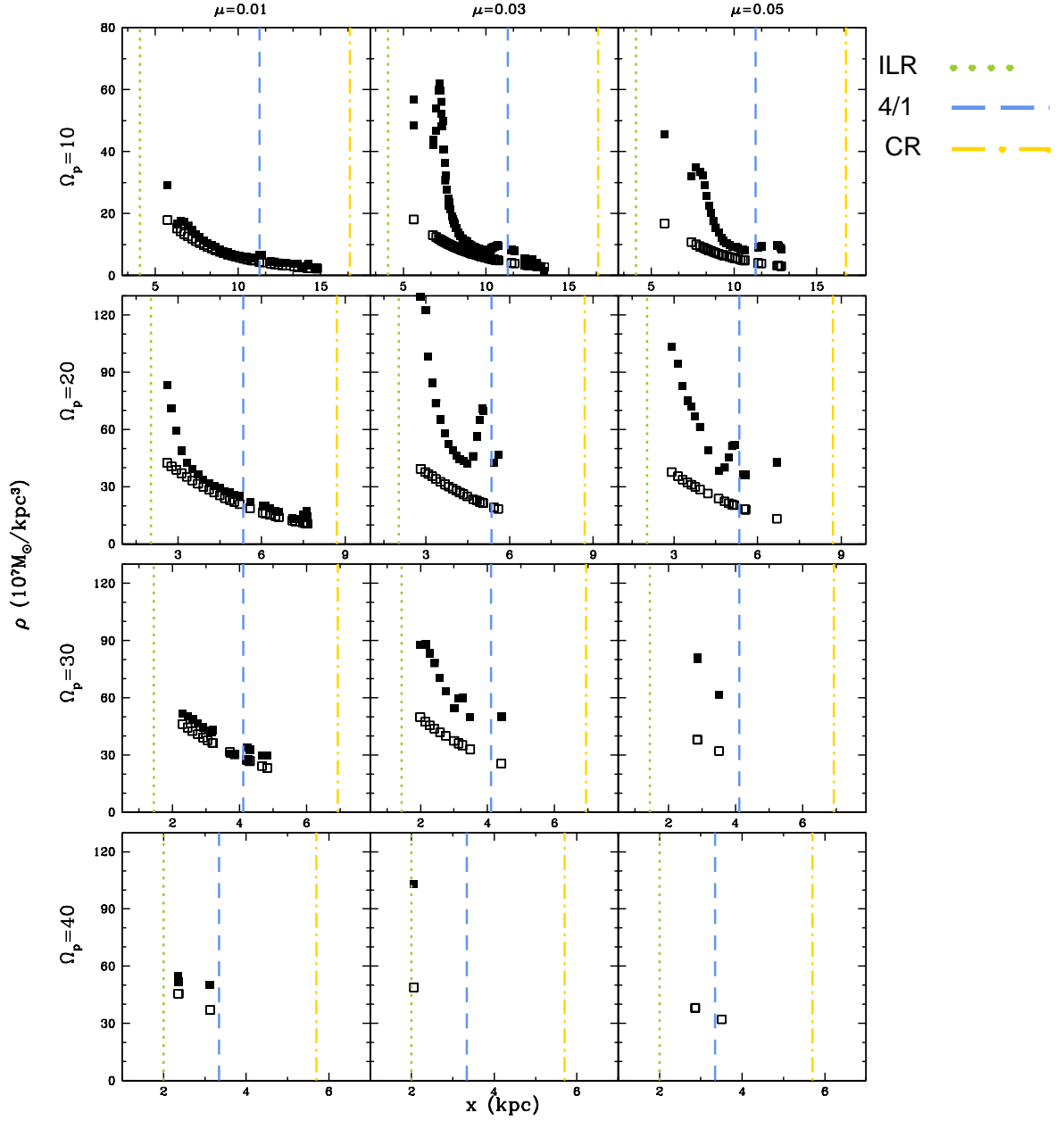Fig. 24.— As in Figure 23, here for an Sb galaxy with $i = 18°$.

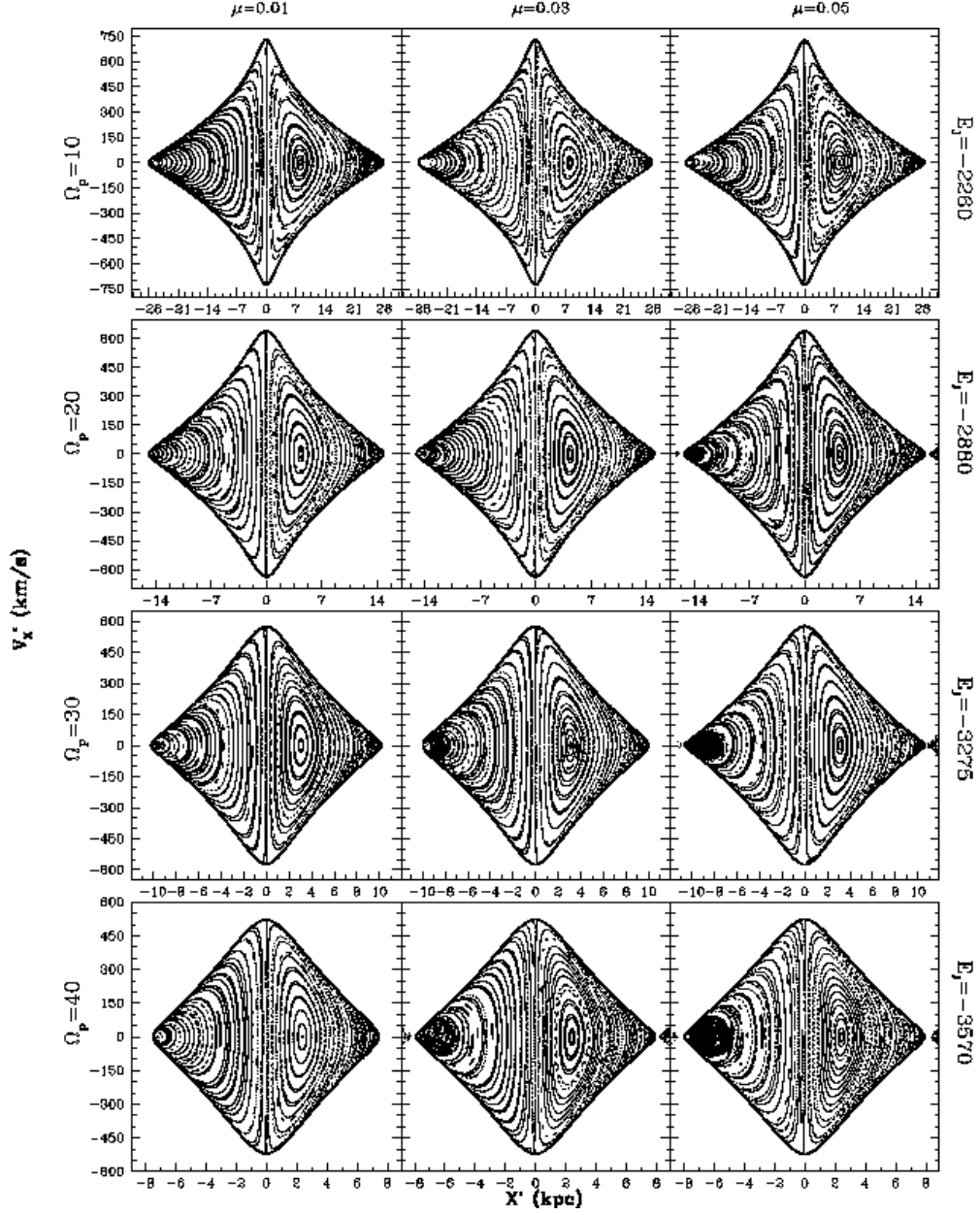Fig. 25.— As in Figure 23, here for an Sc galaxy with $i = 25°$.

Fig. 26.— Phase-space diagrams for an Sa galaxy with $i = 7°$. Here a more extended interval of values for Ω_p is considered, compared with that employed in Section 3.1. The values of the Jacobi energy, μ, and Ω_p, are given at the right, top, and left, respectively.
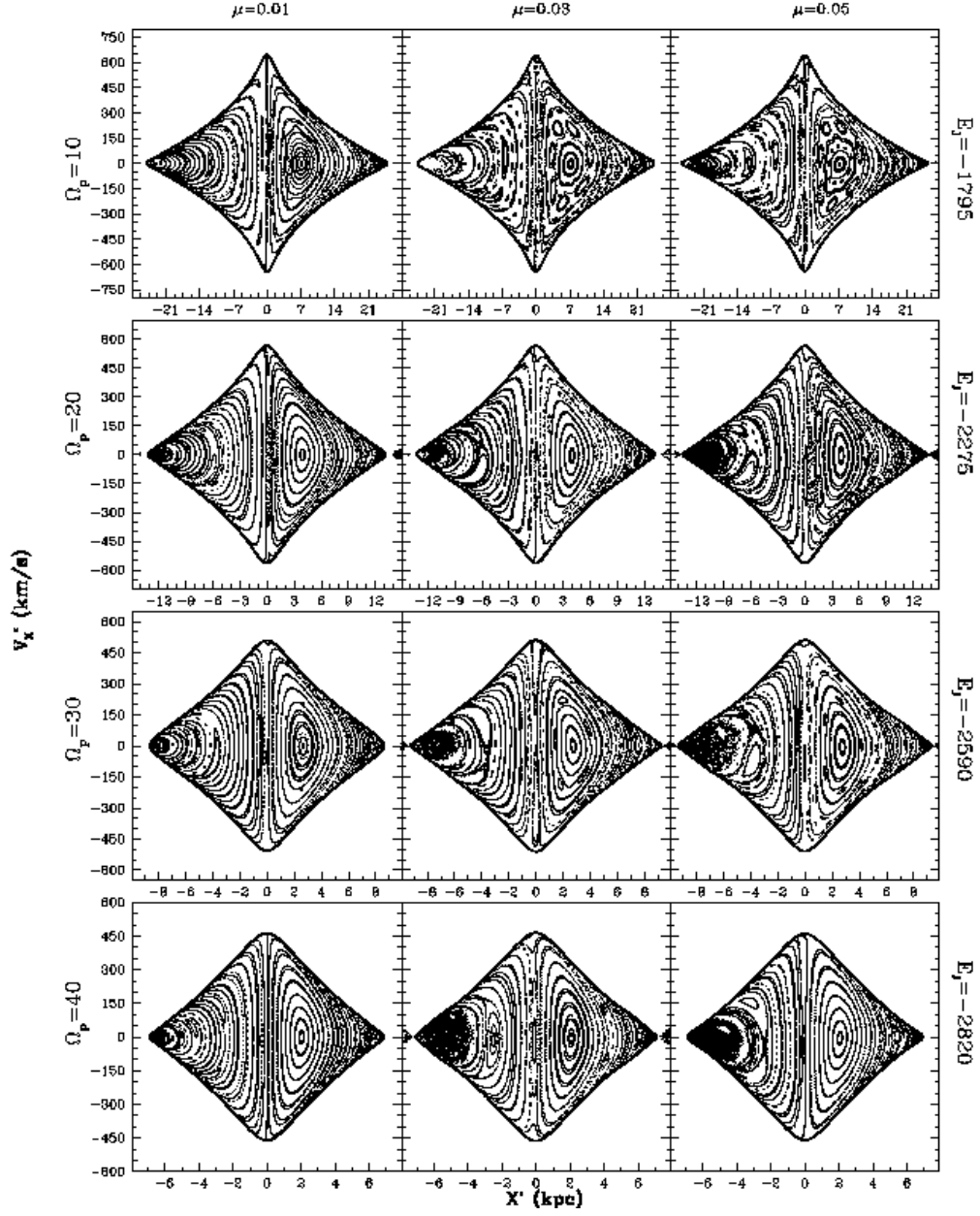
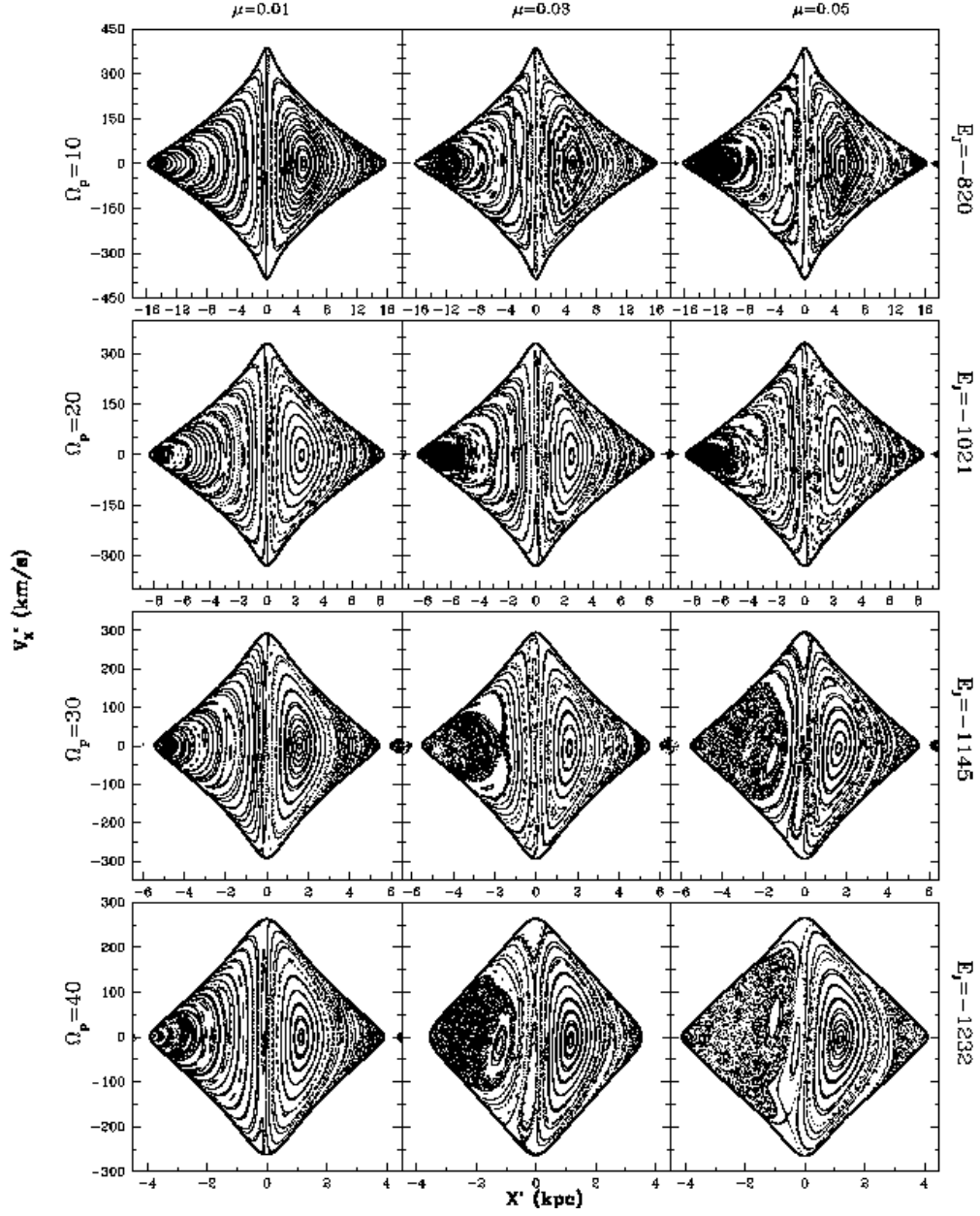Fig. 27.— As in Figure 26, here for an Sb galaxy with $i = 18°$.

Fig. 28.— As in Figure 26, here for an Sc galaxy with $i = 25°$.

insensitive to the angular speed (although it is important because this defines the extension of the spiral arms). With our analysis, we set a limit to Ω_p for each morphological type taking into account the three parametes: for an Sa galaxy, $i \lesssim 7°$, $\Omega_p \sim 40\,\mathrm{km\,s^{-1}\,kpc^{-1}}$, and $\mu \lesssim 0.03$; for an Sb galaxy, $i \lesssim 18°$, $\Omega_p \sim 30\,\mathrm{km\,s^{-1}\,kpc^{-1}}$, and $\mu \lesssim 0.03$; and for an Sc galaxy, $i \lesssim 25°$, $\Omega_p \sim 25\,\mathrm{km\,s^{-1}\,kpc^{-1}}$, and $\mu \lesssim 0.01$. For laeger values, there are not enough periodic orbits to provide support to the spiral arms. These limits for i, Ω_p, and μ are only examples. In the following section we provide a general analysis.

Regarding chaotic behavior, with Poincaré diagrams we also found a maximum value for μ, before chaos becomes pervasive destroying all the main periodic orbits which give support to spiral arms. As we found for the ordered case, the maximum limit of Ω_p is linked to i and μ. An example of the limits for Ω_p depending on i with $\mu = 0.05$ are: for an Sa galaxy with $i \lesssim 7°$, $\Omega_p \sim 40\,\mathrm{km\,s^{-1}\,kpc^{-1}}$; for an Sb galaxy with $i \lesssim 18°$, $\Omega_p \sim 40\,\mathrm{km\,s^{-1}\,kpc^{-1}}$; and for an Sc galaxy with $i \lesssim 25°$, $\Omega_p \sim 30\,\mathrm{km\,s^{-1}\,kpc^{-1}}$.

4. Limits to Parameters for Plausible Dynamical Models for Spiral Arms

Considering the analysis of the effect of the pitch angle that was performed in Paper I, and with the examples obtained in Section 3 concerning the effects of the mass and angular speed of the spiral arms, in this section we present an extended analysis increasing the number of values studied of the parameters i and μ in normal spiral galaxies. We study the ordered and chaotic behavior on the galactic plane, through periodic orbits, maxima density response and Poincaré diagrams. We present two maximum limits for these parameters. The first of them is regarding periodic orbits and density response, where the imposed spiral arms are supported by the density response; this could tell us about the nature of spiral arms: if they are transient or long-lasting. The second limit is a detailed analysis based on phase space diagrams (regardless the spiral arms nature), before the chaotic behavior becomes pervasive dominating all available phase space, and destroying all orbital support.

In Paper I and in Pérez-Villegas et al. (2012) we presented a deep study of the effects of the pitch angle on normal spiral galaxies. The purpose of that study was to provide the values of the pitch angle in galaxies that produced transient or long-lasting galactic models (assuming typical masses for the axisymmetric background potential for disk galaxies from Sa to Sc morphological types). In those studies we considered only the effect of the pitch angle, keeping fixed the mass and angular speed of the spiral arms.

In Figure 29 we summarize our results. First we present a 3×3 mosaic, that shows the maxima values of μ to obtain long-lasting spiral arms, in Sa, Sb, Sc galaxies, depending on the pitch angle i and angular speed Ω_p. Beyond these values the spiral arms would be considered as transient features.

Based in the detailed phase-space orbital study presented in Pérez-Villegas et al. (2012) and
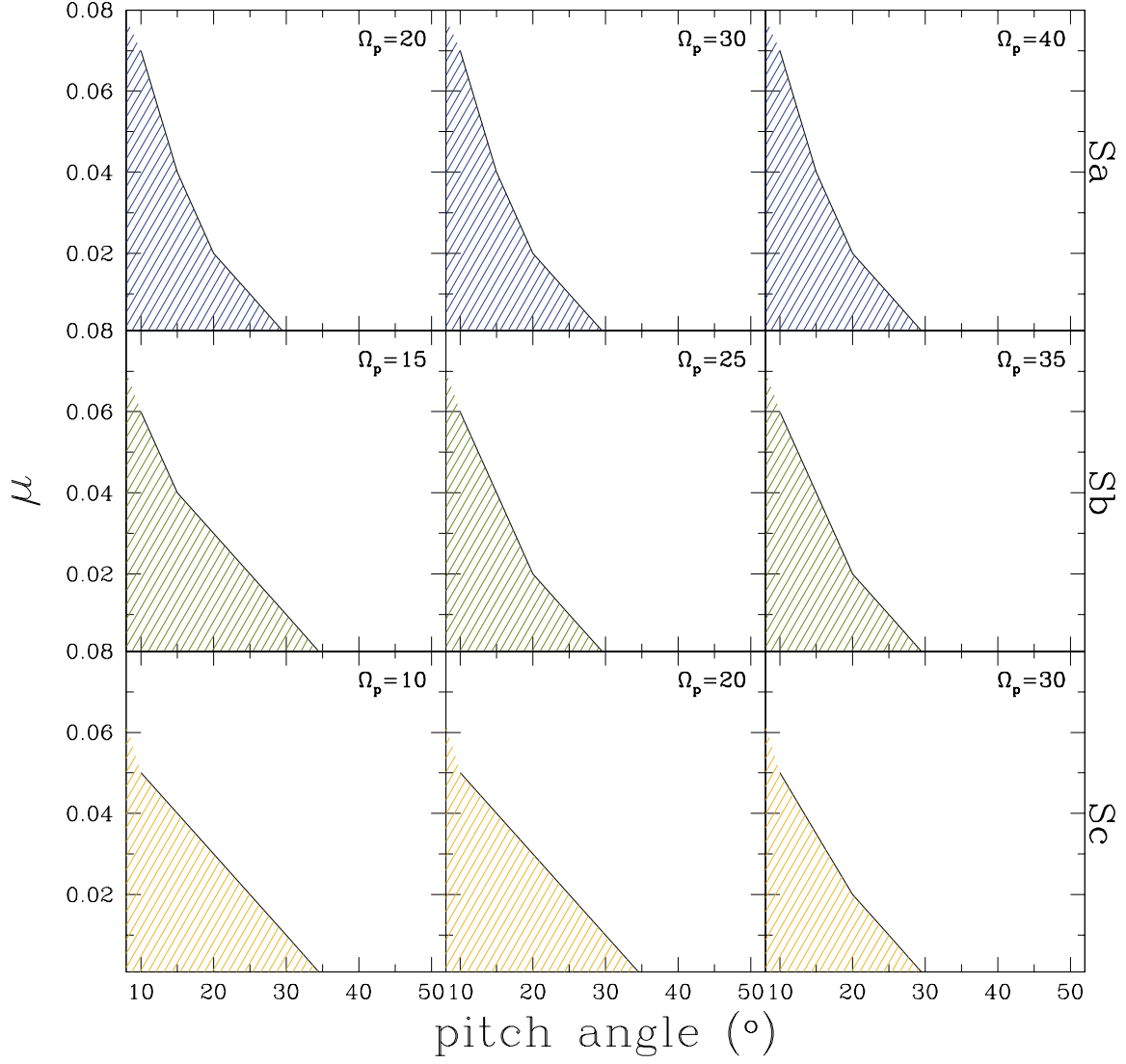
Fig. 29.— Dynamically plausible models for Sa (top line), Sb (middle line), and Sc (bottom line) galaxies. The shaded regions provide the parameters to construct long-lasting spiral arms models in the scheme presented in this work. Spiral arms with parameters outside the shaded regions, would most likely act as transient features.

Paper I, concerning the restriction of the pitch angle given by the chaotic behavior in normal spiral galaxies, here we present maximum values for structural and dynamical parameters of spiral arms such as pitch angle, mass, and angular speed, before the chaotic behavior dominates the available phase-space destroying the main stable periodic orbits. Large-scale structures such as spiral arms are not expected to appear in galaxies where chaotic behavior dominates completely (Voglis et al. 2006); however, confined chaotic orbits may provide some support to spiral arms (Patsis & Kalapotharakos 2011; Kaufmann & Contopoulos 1996; Contopoulos & Grosbøl 1986), up to a certain point, prior to the destruction of all phase space surrounding the periodic orbits that give the shape to spiral arms.

In Figure 30 we present a 3×3 mosaic; each panel shows permitted values of μ and pitch angle i, depending on morphological type and angular speed, before chaos dominates. For values of the spiral arm parameters smaller than those given by the continuous lines, the chaotic behavior may be important, but it is still confined by stable quasiperiodic orbits. For values lager than these limits, the chaotic behavior becomes pervasive destroying all the available prograde phase-space.

5. Discussion and Conclusions

With the use of a family of models observationally motivated to simulate typical Sa, Sb and Sc spiral galaxies, that includes a bisymmetric density-based spiral arms potential model, we perform an extensive analysis of the stellar dynamical effects of spiral arms on galactic disks. The spiral arms model is a self-gravitating three-dimensional potential constructed with individual oblate spheroids (as bricks in a building); this means that the model produces a density based force field (i.e. a more physical model, instead of an *ad hoc* mathematical fit), which means in turn that the potential responds for example to changes on the structure such as a larger pitch angle that naturally produces that disk particles feel a more aggressive effect (i.e. the attack angle for particles is larger the larger the pitch angle is).

In this work, we have extended the studies of Paper I (devoted only to pitch angle effects), to the effects of the spiral arm strength (mass of the spiral arms), its angular speed and pitch angle all together. For all morphological types, we varied the mass of the spiral arms within approximately 1 to 10% of the mass of the disk, and its angular speed from 10 to $60 \, \mathrm{km \, s^{-1} \, kpc^{-1}}$. In Sa, Sb and Sc galaxies, pitch angle employed values were $7°$ to $20°$, $10°$ to $20°$, and $15°$ to $30°$, respectively.

As in paper I, we present two sets of restrictions different in nature for spiral arms parameters. One is based on ordered dynamical behavior and the second on chaotic behavior. Restrictions based on ordered behavior, provide us a tool based on orbital support for the spiral arms that refers to their transient vs. long-lasting nature. The second set of restrictions, based on chaotic behavior, represents the limits beyond which, spiral arms are no longer feasible.

For the first limit, we produced an orbital study based on periodic orbits and computed the maxima density response comparing it with the imposed potential to produce a set of plausible
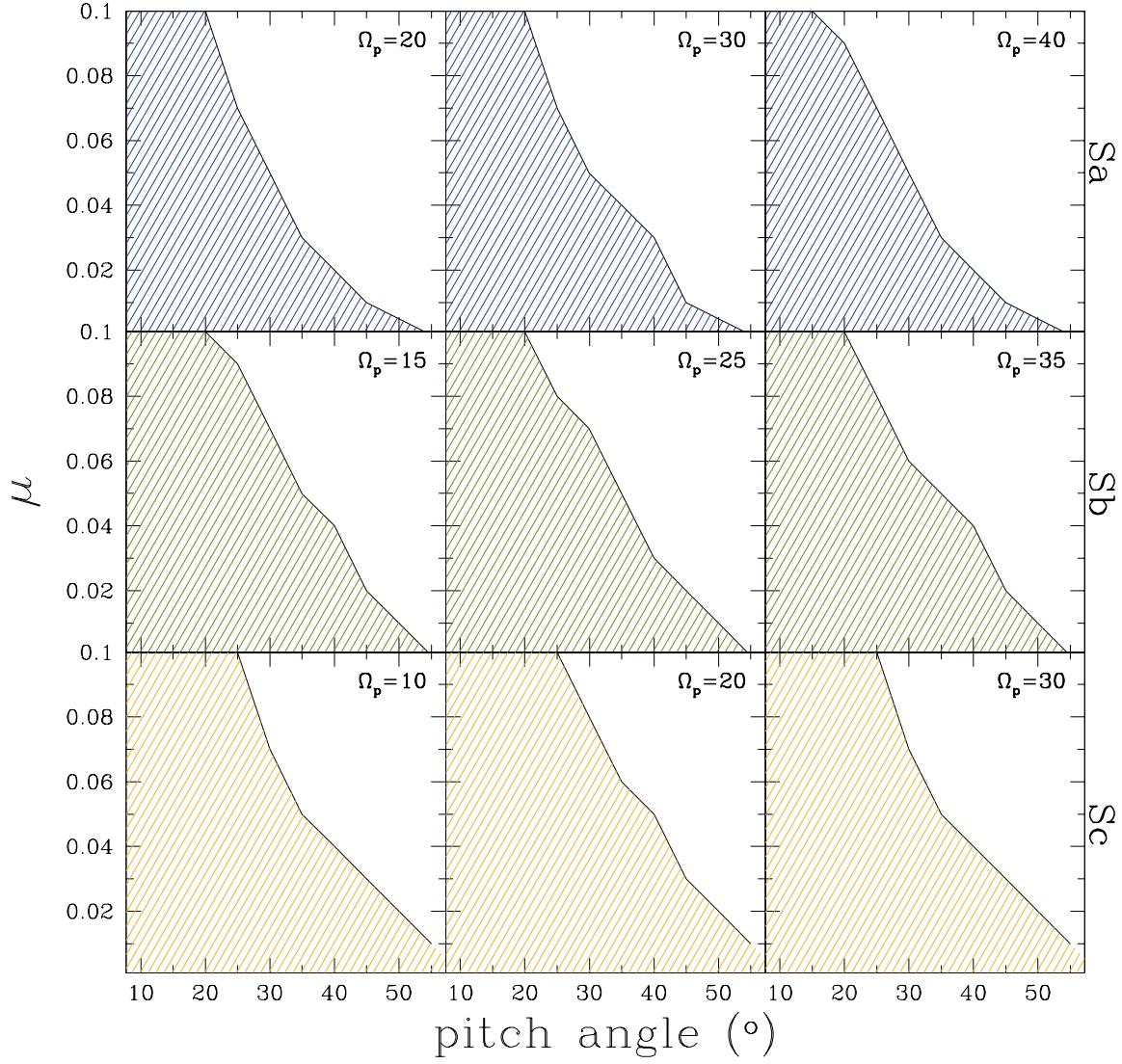
Fig. 30.— Models for Sa (top line), Sb (middle line), and Sc (bottom line) galaxies. The solid line is the maximum limit for the spiral arms models before the domain of chaotic behavior. Parameters for spiral arms on the shaded regions, would be dynamically plausible (independently of their likely transient nature).

models for spiral galaxies with more probable long-lasting spiral arms. In this case we find that the mass of the spiral arms, M_{sp}, should decrease with the increase of the pitch angle i; if i is smaller than $\sim 10°$, M_{sp} can be as large as $\sim 10\%$, $\sim 7\%$, $\sim 5\%$ of the disk mass, for Sa, Sb, and Sc galaxies, respectively. If i increases to $\sim 25°$, M_{sp} is around 1% of the mass of the disk for all morphological types. For values larger than these limits, spiral arms would be transient features.

For the second limit, we produced a phase-space study with Poincaré diagrams, based on chaotic orbital behavior. We seek the parameters of the spiral arms prior to the domain of chaos that destroys all orbital support for the arms. In this case we also found that M_{sp} should decrease with the pitch angle i. If i is smaller than $\sim 20°$, $\sim 25°$, and $\sim 30°$, for Sa, Sb, and Sc galaxies, respectively, then M_{sp} can be up to $\sim 10\%$ of the mass of the disk. If the corresponding i is around $\sim 40°$, $\sim 45°$, and $\sim 50°$, then M_{sp} is 1%, 2% and 3% of the mass of the disk. Beyond these values, chaos dominates all the available phase-space prograde region, destroying the main periodic and the neighboring quasiperiodic orbits.

All the structural and dynamical parameters of the spiral arms play an important role in the orbital dynamics. We found however that the parameter that seems to affect the most the stellar dynamics is the pitch angle since this presents a wide range of possible observational values, unlike the case of the mass (or density contrast), and angular velocity. Within the typical values of the spiral arms angular speed ($\sim 15 - 40\,\mathrm{km\ s^{-1}\,kpc^{-1}}$), obtained from observations and theory, the chaotic orbital dynamical response does not seem to be extremely sensitive.

With all the performed simulations we summarize our results, which are separated according to the two restrictions based on ordered or chaotic orbital behavior:

Restrictions based on ordered orbital behavior: The nature of spiral arms, transient or long-lasting.

- If the maxima density response (at all radii), produced by periodic orbital crowding, support the imposed potential of the spiral arms, i.e. if the arms are orbitally self-consistent at a first approximation, they are more prone to be long-lasting structures; otherwise, the spiral arms would be transient structures.

- Considering the combination of all parameters studied in this work for the spiral arms, we present Table 3. The table shows for different types of galaxies, the spiral arms persistence based on orbital support.

- All the parameters that characterize the spiral arms combined, have to do with the orbital support. From these, due to the wide range of values that can take in all galaxies, the one with more effect on stellar and gas dynamics seems to be the pitch angle.

Restrictions based on chaotic orbital behavior: The destruction of spiral arms.

Table 2.   Resonance Positions

Ω_{p} (km s^{-1} kpc^{-1})	Sa ILR	Sa 4/1 (kpc)	Sa CR	Sb ILR	Sb 4/1 (kpc)	Sb CR	Sc ILR	Sc 4/1 (kpc)	Sc CR
10	9.93	20.25	30.23	8.62	17.74	26.13	4.0	11.32	16.78
15	6.46	13.83	20.53	5.13	12.18	17.88	2.71	7.44	11.49
20	4.45	10.5	15.66	3.52	9.22	13.70	2.03	5.35	8.63
25	3.0	8.44	12.69	2.29	7.34	11.14	1.5	4.11	6.94
30	3.0	7.04	10.6	2.0	6.04	9.38	1.5	3.34	5.7
35	3.0	6.02	9.21	2.0	5.11	8.08	1.5	2.83	4.8
40	3.0	5.24	8.1	2.0	4.40	7.0	1.5	2.45	4.12
50	3.0	4.07	6.51	2.0	3.42	5.64	1.5	1.92	3.19
60	3.0	3.21	5.4	2.0	2.74	4.65	1.0	1.55	2.6

Table 3.   Results based on ordered orbital behavior

Galactic type	Ω_{sp} (km s^{-1} kpc^{-1})	Pitch angle (^{o})	$\mu = M_{\mathrm{sp}}/M_{\mathrm{D}}$	Spiral arm persistence
Sa	$20 \lesssim \Omega_{\mathrm{sp}} \lesssim 40$	$\lesssim 10$	$\lesssim 0.07$	Long-lasting
		$\lesssim 20$	$\lesssim 0.02$	Long-lasting
		$\gtrsim 10$	$\gtrsim 0.08$	Transient
		$\gtrsim 20$	$\gtrsim 0.03$	Transient
Sb	$15 \lesssim \Omega_{\mathrm{sp}} \lesssim 35$	$\lesssim 15$	$\lesssim 0.04$	Long-lasting
		$\lesssim 25$	$\lesssim 0.02$	Long-lasting
		$\gtrsim 15$	$\gtrsim 0.05$	Transient
		$\gtrsim 25$	$\gtrsim 0.03$	Transient
Sc	$10 \lesssim \Omega_{\mathrm{sp}} \lesssim 30$	$\lesssim 15$	$\lesssim 0.04$	Long-lasting
		$\lesssim 30$	$\lesssim 0.01$	Long-lasting
		$\gtrsim 15$	$\gtrsim 0.05$	Transient
		$\gtrsim 30$	$\gtrsim 0.02$	Transient

- The main parameters that determine the destruction of spiral arms are their pitch angle and mass, both directly related to the force amplitude. The destroying effect of their angular speed is slight. Table 4 shows the combination of parameters for which chaotic behavior dominates and destroys the spiral arms.

This study searches for the periodic orbits, that are expected to be the dynamical backbone of a given system. We search for their presence or absence, as a condition for the long-lasting support of large-scale structures in a galaxy. In the same manner, when chaos dominates the phase space (to such extent that even the main periodic orbits are fully destroyed), it is an indication of the demolition of large scale structures, such as spiral arms. Although it is known that confined chaos (trapped between ordered orbits) is able to provide support to structures like spiral arms (Voglis et al. 2006), this can only be true as long as chaos does not become pervasive.

With all the performed simulations we are able to provide a detailed set of plausible galactic models (transient or long-lasting), for normal spiral galaxies, and these idealized galactic models reproduce astrophysical properties of parameters of observed normal spiral galaxies, such as the maximum pitch angles observed in spirals. Although one might wonder about the effect of a bar, given the fact that bars and spiral arms are formed by disk instabilities, likely, even by similar physical processes, the region where a bar grows up on a galaxy and the region where spiral arms grow are dominated by different physical characteristics (e.g. strong differential rotation, mass ratio between spiral arms and the hosting disk, structures size and density etc.). In an ongoing work, we include a galactic bar potential (combined with the spiral arms). Some preliminary results however, show that the presence of a massive bar will change dramatically the orbital self-consistency studies and new and different restrictions will be likely posed.

REFERENCES

Allen, C., & Santillán, A. 1991, Rev. Mexicana Astron. Astrofis., 22, 256

Amaral, L. H., & Lepine, J. R. D. 1997, MNRAS, 286, 885

Antoja, T., Valenzuela, O., Pichardo, B., et al. 2009, ApJ, 700, L78

Antoja, T., Figueras, F., Romero-Gómez, M., et al. 2011, MNRAS, 418, 1423

Athanassoula, E., Bienaymé, O., Martinet, L., & Pfenniger, D. 1983, A&A, 127, 349

Baba, J., Saitoh, T. R., & Wada, K. 2013, ApJ, 763, 46

Block, D. L., Bournaud, F., Combes, F., Puerari, I., & Buta, R. 2002, A&A, 394, L35

Brosche, P. 1971, A&A, 13, 293

Buta, R., Vasylev, S., Salo, H., & Laurikainen, E. 2005, AJ, 130, 523

Cedrés, B., Cepa, J., Bongiovanni, A., et al. 2013, A&A, 560, A59

Combes, F., & Sanders, R. H. 1981, A&A, 96, 164

Contopoulos, G., & Grosbøl, P. 1986, A&A, 155, 11

Contopoulos, G., & Grosbøl, P. 1988, A&A, 197, 83

Davis, B. L., Berrier, J. C., Shields, D. W., et al. 2012, ApJS, 199, 33

D'Onghia, E., Vogelsberger, M., & Hernquist, L. 2013, ApJ, 766, 34

Dobbs, C. L., & Bonnell, I. A. 2006, MNRAS, 367, 873

Donner, K. J., & Thomasson, M. 1994, A&A, 290, 785

Drimmel, R. 2000, A&A, 358, L13

Efremov, Y. N. 1985, Soviet Astronomy Letters, 11, 69

Egusa, F., Kohno, K., Sofue, Y., Nakanishi, H., & Komugi, S. 2009, ApJ, 697, 1870

Elmegreen, D. M., & Elmegreen, B. G. 2014, ApJ, 781, 11

Fathi, K., Beckman, J. E., Piñol-Ferrer, N., et al. 2009, ApJ, 704, 1657

Ferreras, I., Cropper, M., Kawata, D., Page, M., & Hoversten, E. A. 2012, MNRAS, 424, 1636

Foyle, K., Rix, H.-W., Dobbs, C. L., Leroy, A. K., & Walter, F. 2011, ApJ, 735, 101

Fujii, M. S., Baba, J., Saitoh, T. R., et al. 2011, ApJ, 730, 109

Gerhard, O. 2011, Memorie della Societa Astronomica Italiana Supplementi, 18, 185

Grand, R. J. J., Kawata, D., & Cropper, M. 2012a, MNRAS, 426, 167

Grand, R. J. J., Kawata, D., & Cropper, M. 2012b, MNRAS, 421, 1529

Grosbøl, P., & Dottori, H. 2009, A&A, 499, L21

Grosbøl, P. J., & Patsis, P. A. 1998, A&A, 336, 840

Grosbøl, P., Pompei, E., & Patsis, P. A. 2002, Disks of Galaxies: Kinematics, Dynamics and Peturbations, 275, 305

Hubble, E. P. 1926, ApJ, 64, 321

Hubble, E. P. 1936, Realm of the Nebulae, by E.P. Hubble. New Haven: Yale University Press, 1936. ISBN 9780300025002

Junqueira, T. C., Lépine, J. R. D., Braga, C. A. S., & Barros, D. A. 2013, A&A, 550, AA91

Kaufmann, D. E., & Contopoulos, G. 1996, A&A, 309, 381

Kawata, D., Hunt, J. A. S., Grand, R. J. J., Pasetto, S., & Cropper, M. 2014, MNRAS, 443, 2757

Kennicutt, R. 1981, AJ, 86, 1847

Law, D. R., Shapley, A. E., Steidel, C. C., et al. 2012, Nature, 487, 338

Ma, J., Zhao, J.-l., Zhang, F.-p., & Peng, Q.-h. 2000, Chinese Astron. Astrophys., 24, 435

Martinet, L. 1974, A&A, 32, 329

Martínez-García, E. E., & González-Lópezlira, R. A. 2013, ApJ, 765, 105

Martos, M., Hernandez, X., Yáñez, M., Moreno, E., & Pichardo, B. 2004, MNRAS, 350, 47

Meidt, S. E., Rand, R. J., & Merrifield, M. R. 2009, ApJ, 702, 277

Meidt, S. E., Rand, R. J., Merrifield, M. R., Shetty, R., & Vogel, S. N. 2008, ApJ, 688, 224

Merrifield, M. R., Rand, R. J., & Meidt, S. E. 2006, MNRAS, 366, L17

Miyamoto, M., & Nagai, R. 1975, PASJ, 27, 533

Patsis, P. A., Contopoulos, G., & Grosbøl P. 1991, A&A, 243, 373

Patsis, P. A., & Kalapotharakos, C. 2011, Memorie della Societa Astronomica Italiana Supplementi, 18, 83

Pérez-Villegas, A., Pichardo, B., Moreno, E., Peimbert, A., & Velázquez, H. M. 2012, ApJ, 745, L14

Pérez-Villegas, A., Pichardo, B., & Moreno, E. 2013, ApJ, 772, 91

Pichardo, B., Martos, M., Moreno, E., & Espresate, J. 2003, ApJ, 582, 230

Pizagno, J., Prada, F., Weinberg, D. H., et al. 2005, ApJ, 633, 844

Quillen, A. C., Dougherty, J., Bagley, M. B., Minchev, I., & Comparetta, J. 2011, MNRAS, 417, 762

Roca-Fàbrega, S., Valenzuela, O., Figueras, F., et al. 2013, MNRAS, 432, 2878

Roškar, R., Debattista, V. P., Quinn, T. R., & Wadsley, J. 2012, MNRAS, 426, 2089

Sánchez-Gil, M. C., Jones, D. H., Pérez, E., et al. 2011, MNRAS, 415, 753

Scarano, S., & Lépine, J. R. D. 2013, MNRAS, 428, 625

Scarano, S., Jr., Lépine, J. R. D., & Marcon-Uchida, M. M. 2011, MNRAS, 412, 1741

Seigar, M. S., Bullock, J. S., Barth, A. J., & Ho, L. C. 2006, ApJ, 645, 1012

Seigar, M. S., & James, P. A. 1998, MNRAS, 299, 685

Sellwood, J. A. 2011, MNRAS, 410, 1637

Sellwood, J. A., & Carlberg, R. G. 2014, ApJ, 785, 137

Sofue, Y., & Rubin, V. 2001, ARA&A, 39, 137

Speights, J. C., & Westpfahl, D. J. 2012, ApJ, 752, 52

Speights, J. C., & Westpfahl, D. J. 2011, ApJ, 736, 70

Tsoutsis, P., Efthymiopoulos, C., & Voglis, N. 2008, MNRAS, 387, 1264

van den Bergh, S. 2002, PASP, 114, 797

Voglis, N., Stavropoulos, I., & Kalapotharakos, C. 2006, MNRAS, 372, 901

Wada, K., Baba, J., & Saitoh, T. R. 2011, ApJ, 735, 1

Weiner, B. J., & Sellwood, J. A., 1999, ApJ, 524, 112

Weinzirl, T., Jogee, S., Khochfar, S., Burket, A., & Kormendy, J. 2009, ApJ, 696, 411

Yano, T., Kan-Ya, Y., & Gouda, N. 2003, PASJ, 55, 409

Zhang, X. 1998, ApJ, 499, 93

Table 4.   Results based on chaotic behavior

Galactic type	Parameter			
	Ω_{sp} ($\mathrm{km\ s^{-1}\,kpc^{-1}}$)	Pitch angle (^{o})	$\mu = M_{\mathrm{sp}}/M_{\mathrm{D}}$	Chaos predominates
Sa	$20 \lesssim \Omega_{\mathrm{sp}} \lesssim 40$	$\lesssim 25$	$\lesssim 0.09$	No
		$\lesssim 45$	$\lesssim 0.02$	No
		$\gtrsim 25$	$\gtrsim 0.07$	Yes
		$\gtrsim 45$	$\gtrsim 0.01$	Yes
Sb	$15 \lesssim \Omega_{\mathrm{sp}} \lesssim 35$	$\lesssim 35$	$\lesssim 0.07$	No
		$\lesssim 45$	$\lesssim 0.02$	No
		$\gtrsim 35$	$\gtrsim 0.05$	Yes
		$\gtrsim 45$	$\gtrsim 0.02$	Yes
Sc	$10 \lesssim \Omega_{\mathrm{sp}} \lesssim 30$	$\lesssim 40$	$\lesssim 0.05$	No
		$\lesssim 50$	$\lesssim 0.03$	No
		$\gtrsim 40$	$\gtrsim 0.04$	Yes
		$\gtrsim 50$	$\gtrsim 0.02$	Yes